Project Title: Novel Electro-Deoxygenation Process for Bio-oil Upgrading

Sponsoring Office: Depart of Energy – Energy Efficiency & Renewable Energy
Award No. DE-EE0006288

Period of Performance: 09/30/2013 – 03/31/2018

Principal Investigator: Dr. S. (Elango) Elangovan

Key Personnel and Project Partners

Mr. Douglas Elliott	Pacific Northwest National Laboratory
Mr. Daniel (Miki) Santosa	Pacific Northwest National Laboratory
Dr. Sabrina Spatari	Drexel University
Dr. Mukund Karanjikar	Technology Holding LLC

Contributors

Joseph Hartvigsen ((OxEon Energy)	Insoo Bay (Ceramatec)
Evan Mitchell (OxEon Energy)	Dennis Larson (OxEon Energy)
Dr. Pieter Billen (University of Antwerp)	Tyler Hafen (OxEon Energy)
Dr. Yetunde Sorunmu (Drexel University)	Mr. Benjamin Q. Roberts (PNNL)
Michelle Torelli (Drexel University)	Mr. Igor V. Kutnyakov (PNNL)

Technical Point of Contact
Dr. S (Elango) Elangovan
Vice President – Research
OxEon Energy, LLC
257 River Bend Way
North Salt Lake, UT 84054

Business Point of Contact
Mr. Lyman Frost
Chief Executive Officer
OxEon Energy, LLC
257 River Bend Way
North Salt Lake, UT 84054

June 2018

Acknowledgement

OxEon team acknowledges the financial support of DOE-BETO. Many former employees of Ceramatec and current employees of OxEon Energy made valuable contribution to the technical success of the project. PNNL acknowledges the contribution of Dr. Daniel T. Howe (PNNL) and Stephen Deutch (NREL) with the design of the electrostatic precipitator and overall improvement of product recovery, Dr. Huamin Wang (PNNL) for help with discussion of the catalysis aspect of the project and discussion of the final report and finally Marie Swita (PNNL) and Dr. Teresa Lemmon (PNNL) for help with analyzing the liquid products.

This material is based upon work supported by the Department of Energy's Office of Energy Efficiency and Renewable Energy under the Bioenergy Technologies Office, Award Number EE0006288.

Table of Contents

List of Figures

List of Tables

Executive Summary

Biomass is a potential source of renewable fuel. Bio-oil produced by fast pyrolysis is a prospective option to replace fossil fuels for transportation. However, bio-oil needs to be upgraded to remove its high oxygen and water content, and acidity to produce useful fuels. The upgrading of bio-oil is generally accomplished by hydrodeoxygenation (HDO) using hydrogen. The instability of bio-oil poses a major challenge in transportation to central upgrading facility.

An electro-deoxygenation (EDOx) process was evaluated to fully or partially deoxygenate bio-oil using solid oxide electrolysis process.* This device uses an oxygen ion conducting membrane which under an applied electric potential removes oxygen in the form of an ion and transports it to the opposite side of the membrane where it is released as oxygen molecule. When water is present in the bio-oil vapor, the process generates in situ hydrogen to facilitate deoxygenation over the electrode that functions as catalyst.

The significant features of the EDOx process are:

- Minimal or No external hydrogen needed,
- The electricity can be obtained locally from co-gen facilities that use renewable sources and/or from existing infrastructure;
- Additionally, partial or complete removal of the oxygen from the pyrolyzed material stabilizes the hydrocarbon product for transport;
- Deoxygenation will also result in a product with none of the acidity problems typical of pyrolysis oil;

As oxygen is removed as $O_{2(g)}$ and not as oxides of carbon, EDOx can theoretically be very high in carbon and hydrogen efficiency;

- If the production of char is minimized in the pyrolysis step, the entire system can achieve high atom efficiencies;
- EDOx has the potential to be integrated directly with a pyrolysis reactor and thus, the overall system will operate at atmospheric pressure thereby obviating the need for expensive pressure vessels.
- Modularity of both the fast pyrolysis and EDOx units allows a smaller integrated facility to be economically attractive, increasing both the flexibility for deployment and broadening the potential customer base.
- Oxygen can be recovered as a co-product which will aid in overall process economics.

A series of tests conducted using model compounds and aqueous fraction of bio-oil demonstrated the potential of the process. The project culminated in an integrated test wherein a slip stream of bio-oil from a fast pyrolysis unit was introduced to a solid oxide stack. integrated testing of stack-cell EDOx reactor with the fast pyrolysis system successfully demonstrated conversion of pyrolysis oil vapor to an upgraded liquid product and displayed a significant level of deoxygenation. As a result, correlation of pyrolysis oil deoxygenation with the stack current (Amperes) was made. Liquid and gas yields were also estimated, and product analysis was done to provide a clear baseline performance for future development of the EDOx process. In addition to the experimental work and results, computational chemistry work at PNNL demonstrated the feasibility of deoxygenation via dehydroxylation of the oxygenates (Guaiacol $\rightarrow$ Phenol) present in the pyrolysis vapor by using DFT (Density Functional Theory). This was also confirmed by ^{13}C NMR analysis of the liquid product with the decrease of carbon-hydroxyl (C-OH) group in the product. Additional work is required to evaluate new catalytic materials and process optimization schemes for improvement of the deoxygenation process to produce hydrocarbon fuels and chemicals.

* The project was initially awarded to Ceramatec, Inc. and novated to OxEon Energy.

Much of the work used conventional solid oxide cells that used thick electrolyte and electrodes that were optimized for higher temperature operation than the pyrolysis process. The high electrolyte resistance and the lower operating temperature limited the maximum current achievable and therefore the amount of oxygen removed from the bio-oil vapors. This project also demonstrated an experimental thin electrolyte cell design that showed improved performance at the lower temperature when tested in a button cell. Thin electrolyte design with its increased performance will reduce the capital cost of the device. With a projected five-fold increase in performance with the use of a thin electrolyte, a stack of 100 cells would theoretically remove nearly all oxygen present in bio-oil. More research is also needed to experimentally evaluate fuel electrode (cathode) material with higher catalytic activity and selectivity towards preferred deoxygenated species and oxygen electrode material with lower polarization losses. Furthermore, this project will benefit from demonstration of a larger scale stack that can receive all of the pyrolysis vapor for deoxygenation study.

Techno-economic analysis (TEA) and life cycle analysis were also conducted. Results show that the EDOx configurations have lower life cycle GHG emissions of 5 – 8.4 g CO_2 eq. and 7.4 – 11 g CO_2 eq. per MJ of a vehicle operated with diesel and gasoline, respectively compared to HDO (39 gCO_2 eq. per MJ). Furthermore, the EDOx process offers potentially10 times more small-scale pyrolysis upgrading facilities in the U.S. compared to HDO, suggesting that small-scale on-site EDOx processes can reach more inaccessible forest biomass resources.

The plant is designed to use 300 metric tons/day of forest residue to produce 1.1 M gallons per year of gasoline and diesel which is an overall yield of 47 L of fuel produced per dry metric ton of feedstock. The processing steps include:

1. Feedstock collection
2. Fast pyrolysis conversion of feedstock to bio-oil
3. Electrochemical deoxygenation of bio-vapor to produce stable deoxygenated oil
4. Further hydrotreating of electrochemical deoxygenated oil
5. Product separation of deoxygenated oil

The capital cost for the plant is estimated to be $53 million (2015 basis). At an ROI of 10%, the minimum fuels (gasoline and diesel) selling price is $1.89/gal which is competitive with the estimated MFSP of the state of the art HDO technology reported to be between the range of $1.74- $2.04/gal. In addition we project that the revenue from sales of the biofuel product at the estimated MFSP will be $210 million.

Although the MFSP of the EDOx process is relatively competitive with the HDO technology, the EDOx process has the potential to have a lower MFSP if the EDOx reactor can reach its full deoxygenation potential, thereby reducing the hydrogen demand required for further deoxygenation and reduce cost. Therefore, further research can possibly lead to additional cost improvements.

Chapter 1: Electrochemical Deoxygenation Process Development

Background

Production of renewable fuel has been of interest to supplement in the near term and potentially replace petroleum fuel in the long term. Biomass as source of fuel is of interest due to their renewable nature and availability. Bio-oil obtained by fast pyrolysis is one option for producing transportation fuel. However, bio-oil properties such as low heating value, incomplete volatility, acidity, instability, and incompatibility with standard petroleum fuels significantly restrict its application.[1] The undesirable properties of pyrolysis oil result from the chemical composition of bio-oil that mostly consists of different classes of oxygenated organic compounds. The elimination of oxygen is thus necessary to transform bio-oil into a liquid fuel that would be broadly accepted and economically attractive. Comparison of properties of bio-oil and petroleum fuel is shown in Table **1**.[2]

Table 1. **Property Comparison of Bio-oil and Petroleum Fuel**

Characteristic	Fast pyrolysis Bio-oil		Heavy petroleum fuel
Water content, wt%	15-25		0.1
Insoluble solids, %	0.5-0.8		0.01
	Wet	**Dry**	
Carbon, %	39.5	55.8	85.2
Hydrogen, %	7.5	6.1	11.1
Oxygen, %	52.6	37.9	1.0
H/C	2.3	1.3	1.6
O/C	1.0	0.5	0.01
Nitrogen, %	<0.1		0.3
Sulfur, %	<0.05		2.3
Ash	0.2-0.3		<0.1
HHV, MJ/kg	17		40
Density, g/ml	1.23		0.94
Viscosity, cp	10-150 @50ºC		180 @50ºC

Two types of processes that have been used to remove oxygen from organic molecules are catalytic cracking and hydrotreating. The former accomplishes the removal of oxygen in the form of water and carbon oxides using shape-selective catalysts while the latter uses hydrogen to remove oxygen in the form of water. Reviews on catalytic cracking[3] and hydrotreating[4] describe the principles of these processes and provide numerous citations to original studies in those areas. Catalytic cracking, considered a cheaper route, converts oxygenated feedstock to lighter fuel grade fractions. Catalytic cracking accomplishes deoxygenation through simultaneous dehydration, decarboxylation, and decarbonylation reactions occurring in the presence of catalysts. Most of the prior art discusses use of zeolite such as ZSM5 catalysts to perform cracking. Other catalysts such as molecular sieves (SAPOs), mordenite and HY-zeolite are investigated by different researchers.[5] The extent of coking (8-25%), high extent of formation of light ends (gas-phase hydrocarbons) and low quality of final fuel grade products are prohibitive towards a scalable cracking process.[6] All these factors result in carbon and hydrogen loss thereby reducing both carbon and hydrogen efficiencies.

A catalytic reforming approach offers several potential advantages over hydrotreating and catalytic cracking such as no or low need for hydrogen, atmospheric pressure processing, and a possibility of close coupling with pyrolysis that could make the process logistically and economically attractive.

The state of the art in aqueous phase reforming as a route for conversion of pyrolysis oil to transportation fuel is very limited.[7] Catalyst stability in presence of aqueous phase is a significant challenge. Most of the catalysts used for hydrodeoxygenation are some variations of Co-Mo or Ni-Mo impregnated on a support. Many investigators have focused upon alumina as a preferred catalyst support. Others have investigated carbon, silica and zeolite based supports. HDO is considered the leading technology to achieve oxygen removal from bio-oil. HDO consists of contacting the bio-oil with hydrogen at high pressure and high temperature in presence of a catalyst.[8] However, HDO suffers from significant challenges as listed below:

- Coking, which limits the catalyst lifetime.[9]
- Polymerization of various compounds in bio-oil before deoxygenation due to sequential nature of bio-oil productions and catalytic treatment.
- Deactivation of HDO catalysts by the presence of water in the pyrolysis oil. The deactivation occurs by leaching sulfur from active sites since these catalysts are usually sulfided prior to HDO process to alleviate coking.
- Hydrothermally unstable nature of zeolite based catalysts compared to noble metal catalysts, which are cost prohibitive.[10]
- Requirement of significant quantities of hydrogen to remove oxygen. Cost of hydrogen is approximately $1.50 per gallon of product hydrocarbon.
- Economic availability of hydrogen at distributed smaller scale suitable for biomass conversion.
- Significant process exotherm due to high oxygen removal requirement (25% by mass). This will require high recycle rates at commercial scale to manage the heat, which contributes to high processing costs.[11]

Thus, there are numerous challenges that prevent commercialization of bio-oil upgrading to hydrocarbons process. An *alternative economically feasible, hydrogen independent and decentralized process* is required to convert biomass derived pyrolysis oil to refinery ready hydrocarbons. An electrochemical approach to remove oxygen from bio-oil is the focus of this project.

Innovation and Novelty

OxEon Energy[†] in collaboration with Pacific Northwest National Laboratory (PNNL) investigated an electrochemical deoxygenation (EDOx) technology with the potential to economically convert oxygenated oils and/or vapors to a mixture of hydrocarbon products suitable for subsequent fractionation in conventional refineries. Figure 1 shows the working principle of the EDOx unit. The overall system level solution is shown in Figure 2. The EDOx process removes oxygen using electrons (provided via electricity) stoichiometrically. EDOx is carried out in an oxygen ion transporting dense ceramic membrane reactor that selectively removes oxygen as a pure gas (Figure 1). The oxygen is transported as oxygen ions through the membrane upon application of an electric potential across the membrane. The significant features of the device are:

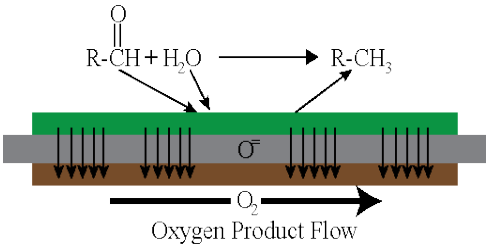

Figure 1. The novel EDOx process to remove oxygen from bio-oil yields hydrocarbons

- No external hydrogen, a cost intensive reagent in refining technologies, is necessary if adequate steam is present and the EDOx cell can sustain adequate electric current to locally produce electrolytic hydrogen;
- The electricity can be obtained locally from co-gen facilities that use renewable sources and/or from existing infrastructure;

[†] The project was initially awarded to Ceramatec, Inc. and novated to OxEon Energy.

- Additionally, partial or complete removal of the oxygen from the pyrolyzed material stabilizes the hydrocarbon product for transport;
- Deoxygenation will also result in a product with none of the acidity problems typical of pyrolysis oil;
- As oxygen is removed as $O_{2(g)}$ and not as oxides of carbon, EDOx can theoretically be very high in carbon and hydrogen efficiency;
- If the production of char is minimized in the pyrolysis step, the entire system can achieve high atom efficiencies;
- EDOx has the potential to be integrated directly with a pyrolysis reactor and thus, the overall system will operate at atmospheric pressure thereby obviating the need for expensive pressure vessels.
- Modularity of both the fast pyrolysis and EDOx units allows a smaller integrated facility to be economically attractive, increasing both the flexibility for deployment and broadening the potential customer base.
- Oxygen can be recovered as a co-product which will aid in overall process economics.

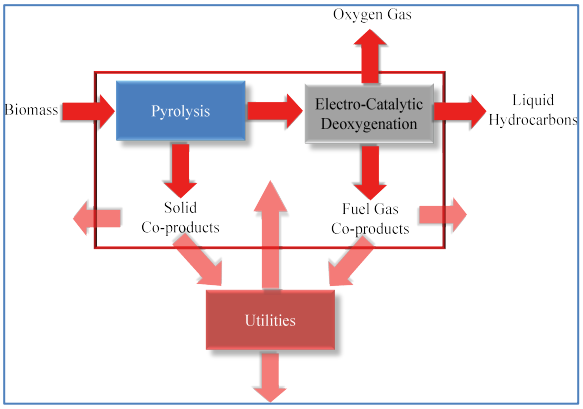

Figure 2. The overall pyrolysis oil to liquid hydrocarbons system without using hydrogen

This system synergistically converts cellulosic biomass and electricity to energy dense liquid fuels. This solves two problems:

1. Biomass has a relatively low energy density and thus is hard to transport for fuel needs, and

2. Electricity is difficult to store which prevents increased utilization of renewable sources of electricity such as solar and wind. If integrated with renewable electricity sources, this system effectively amplifies the energy in biomass with renewable electricity.

The overall pyrolysis-EDOx combination (pyrEDOx) is schematically shown in Figure 2.

Technical Basis

High temperature electrolysis using solid oxide electrolyte cells is an exceptionally efficient means of generation of high purity hydrogen. [12] Co-electrolysis (Figure 3) is fundamentally a variation of high temperature steam electrolysis. An electrical potential is applied across a gas tight and electrically insulating ceramic membrane, having a high conductivity of oxygen ions. Zirconia (ZrO_2), doped with tri-valent cations (e.g. Y_2O_3 to 8 mole%) to stabilize a cubic structure and introduce oxygen vacancy defects, is the most common ceramic electrolyte material for this and the related fuel cell devices. If the potential is greater than the free energy of formation, corrected for local reactant and product partial pressures, an H_2O or CO_2 molecule will decompose as one oxygen atom is transported across the membrane in the form an oxygen ion ($O^{=}$) leaving behind hydrogen or carbon monoxide. However, quantitative analysis of co-electrolysis is significantly more complex than simple steam electrolysis. This is primarily due to the multiple, interacting reactions that occur: steam electrolysis, CO_2 electrolysis, and the reverse shift reaction (RSR): $CO_2 + H_2 \leftrightarrow CO + H_2O$.

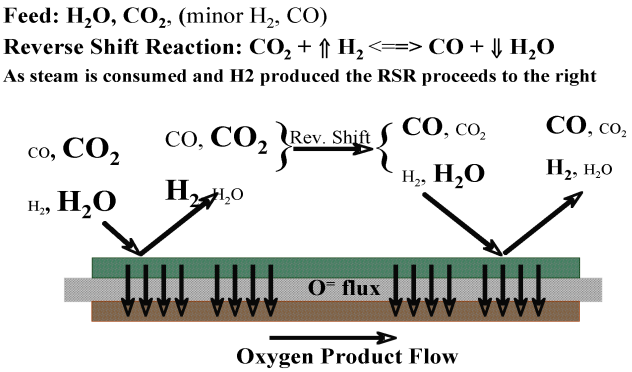

Figure 3. Schematic of high temperature co-electrolysis

Reaction kinetics govern the relative contributions of these three reactions. It is also important to note that the electrolysis reactions are not equilibrium reactions. The electrolyte separates the products from the reactants. However, the RSR is a kinetically fast, near equilibrium reaction at high temperature in the presence of a Ni catalyst. Further, the electrolysis cell cathode is typically a nickel ceramic composite and an effective shift or reforming catalyst. Note that all four species participating in the RSR are present on the cathode as shown in Figure 3.

A similar process scheme can be envisioned for deoxygenation of pyrolysis oil vapor. Similar to electrolysis of CO_2, oxygen can be extracted directly from an oxygenated compound by application of electric potential across a solid oxide cell, or from steam (H_2O molecule), which in turn produces hydrogen. The produced hydrogen then reacts with the oxygenated compound to produce lower oxygenates or even hydrocarbons and water. The extent of reduction is determined by the hydrogen partial pressure and temperature. The possible reactions that can happen in the cathode chamber by hydrogen reduction of pyrolysis vapor resulting in hydrocarbons are shown in

Table 2.

Table 2. Hydrocarbons from Pyrolysis oil

Acids	R-COOH + $3H_2$	→	$RCH_3 + 2H_2O$
Acids	2R-COOH	→	R-R + 2CO2
Aldehydes	R-CHO + $2H_2$	→	$R\text{-}CH_3 + H_2O$
Aldehydes	2R-CHO +$3H_2$	→	$R\text{-}CH_2\text{-}CH_2\text{-}R + 2H_2O$
Ketones	R-CO-R + $2H_2$	→	$R_2CH_2 + H_2O$
Ketones	2R-CO-R' +$3H_2$	→	RR'CH-CHR'R +$2H_2O$
Alcohols	R-CH_2OH + H2	→	$R\text{-}CH_3 + H_2O$
Ethers	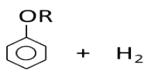	→	
Phenols	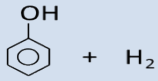	→	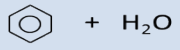

Efficiency Potential of the Process

Theoretically very high carbon and hydrogen efficiency is attainable in the EDOx process provided bio-oil vapor does not produce coke on the electrode layers and the formation of oxides of carbon is limited over the electrode. The high efficiency is possible because oxygen removed in its elemental form and not as a molecule combined with C or H. Energy is required to produce $O_2(g)$, and this energy is supplied by electricity, which is stored in an energy dense liquid hydrocarbon fuel where the hydrogen and carbon come from cellulosic biomass. The EDOx process is based on high temperature electrolysis (HTE) process. The HTE process is endothermic while the resistive loss (i.e. electrical resistance of the membrane and electrodes) is exothermic. A 100% electricity to heating value of product can be achieved by careful selection of the process operating voltage such that the endotherm and exotherm match. This voltage, commonly termed thermal neutral voltage V_{tn} is calculated as:

$$V_{tn} = \frac{\Delta H}{nF}$$

where ΔH is the enthalpy of reaction, n the number of electrons involved and F the Faraday's constant. The team has demonstrated an electrical efficiency of >96% for both steam electrolysis to make hydrogen, and

CO_2 and steam co-electrolysis to make syngas in a 4 kW laboratory module.[13] As in the case of co-electrolysis, the ΔH value for the proposed EDOx process will depend on the relative amounts of various molecules. When a single operating voltage is selected, a distribution of electrical efficiencies will be seen for the process. The overall electrical efficiency can be in the 90% range and the C and H efficiency will also be very high because of the unique features of this process.

Technical Progress

Bio-oil contains a complex set of chemical compositions numbering over 300. It retains a population of carbon, hydrogen, and oxygen similar to that of the original biomass.[14] The liquid fraction consist of complex mixture of oxygenated hydrocarbons with additional moisture from the starting biomass and the reaction products. [15] Major components of bio-oil fall in the category of Hydroxyacetone, Hydroxyacetaldehyde, Acetic Acid, Guaiacols, Sugars, Levoglucosan, Furfural, 2-Furanone.[16]

Model Compound Selection

PNNL supplied the team with a list of model compounds that can be used as surrogates for the bio-oil:

- Acetic acid
- Furfural
- Phenol
- 2-Methyl-2-cyclopenten-1-one
- Acetol (hydroxyacetone)
- Methanol
- Guaiacol (2-methoxyphenol)
- Syringol (2,6-dimethoxyphenol)
- Levoglucosan (anhydroglucose)

Properties of these compounds are given in Table 3.

Table 3. Properties of Model Compounds

Chemical	Form	MP °C	BP, °C	FP, °C	IT, °C	Den	Sol	MW	Formula	Hazard
Acetic Acid	Liq	17	118	ND	45	1.049	misc	60.05	$C_2H_4O_2$	combustible, corrosive, toxic
Acetol (hydroxyl-acetone)	Liq	-17	145	56	ND	1.08	ND	74.08	$C_3H_6O_2$	fire, explosion, skin contact
Levoglucosan (anhydroglucose)	powder	183	ND	ND	ND	ND	ND	162.14	$C_6H_{10}O_5$	
Furfual	Liq	-36	162	60	315	1.16	sol	96.08	$C_5H_4O_2$	toxic, flammable, carcinogen
2-methyl-2cyclopenten-1-one	Liq	ND	160	49	ND	0.979	ND	96.13	C_6H_8O	combustible
Phenol	Solid	41	182	79	715	1.071	ND	94.11	C_6H_6O	toxic, mutagen, skin corrosion, inhalation toxicity
Guaiacol (2-methoxyphenol)	Crys-talline	27	205	82	ND	1.129	ND	124.14	$C_7H_8O_2$	toxic, irritant
Syringol (2,6-dimethoxyphenol)	Solid	53	261	140	ND	ND	ND	154.16	$C_8H_{10}O_3$	harmful if swallowed, irritant, dust inhalation
Methanol	Liq	-8C	64.7	9.7	455	0.791	misc	32.04	CH_4O	flammable, toxic

MP: Melting point, BP: Boiling Point, FP: Flash Point,; IT: Ignition Temperature; Den: Density; Sol: Solubility in Water; MW: Mol Wt

Device Design

In an electrochemical cell, under an applied voltage, the oxygen from either the oxygenated organic compound or the steam present is ionized. The oxygen ion is transported through the ceramic membrane to the air electrode and released in the form of oxygen molecule. The remaining hydrocarbon radical could react with the hydrogen (in the form of proton) left from the electrolysis of water to form deoxygenated hydrocarbon. The radical could also combine with other similar radicals or its fragments to form dimers or other more complex hydrocarbons that have potentially reduced oxygen content. The type of hydrocarbon

formed will depend on the catalytic properties of the fuel electrode (cathode), type of oxygenated compound, and cell temperature.

Two types of electrochemical cell designs were used for deoxygenation testing. The first type of cells used were of button cell type that is approximately a 1.25" electrolyte disc with an anode (air electrode) and cathode (fuel electrode) printed and sintered on each face of the electrolyte. The button cell is then manifolded on the fuel electrode side so that vapors of model compound can be fed to the fuel electrode. The air electrode where oxygen, transported from the oxygenated bio-oil compound and steam in the feed, is evolved is open to the ambient air. In a commercial system opportunity exists to collect the transported high purity oxygen as a valuable by-product. A photograph of a manifolded button cell is shown in Figure 4.

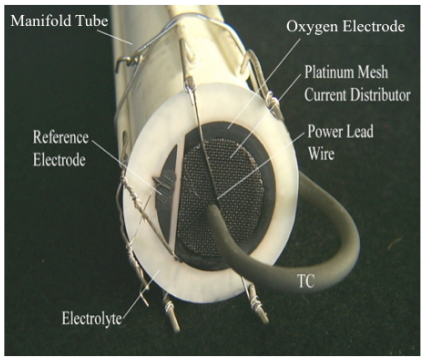

Figure 4. Photograph of Electrochemical Button Cell

The second type of cells consisted of multi-cell stack of larger foot print. The electrolyte is of 10 cm x 10 cm in size with an electrode area typically of 45 to 64 cm^2. Figure 5 shows a schematic of the major materials used in the construction of a stack. In addition to metallic bipolar plats, the stack has additional current collection layers that electrically connect the electrode to the metallic corrugated plates. One difference between the stack and button cells stems from the flow configuration of the bio oil vapor. In the case of a button cell the feed stream flows perpendicular to the electrode area and the product stream moves in a counter current fashion within the same chamber, essentially creating continuously stirred tank reactor (CSTR) conditions. In a stack, the inlet vapors move parallel to the electrode surface from one end to the opposite end in a plug flow fashion. The stack flow allows for much longer residence time and avoids mixing of fresh inlet and product stream. A photograph of a 10-cell stack is shown in Figure 6.

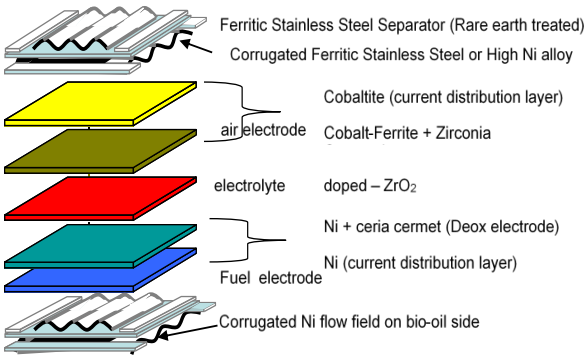

Figure 5 Schematic of Materials Construction

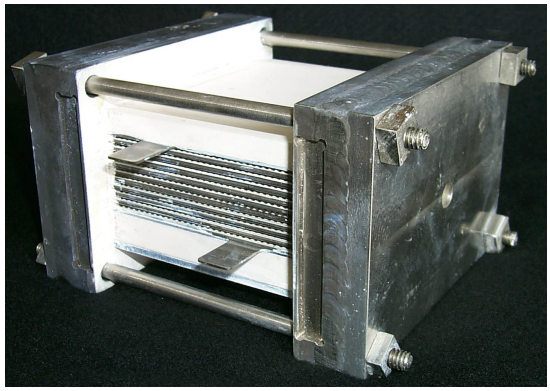

Figure 6. Photograph of Electrochemical Stack

Experimental Set up

In conventional steam electrolysis tests, steam is fed to the cathode chamber by bubbling a mixture of nitrogen and hydrogen through a heated water bubbler. When a mixture of carbon dioxide and steam needs to be electrolyzed, CO_2 is also co-fed through the heated water bubbler. For model bio-oil components with varying boiling points, a more detailed feed system needs to be used, as shown in Figure 7. Mass flow controllers, bio-oil vaporizers, chillers, and condensers were included in the test set up.

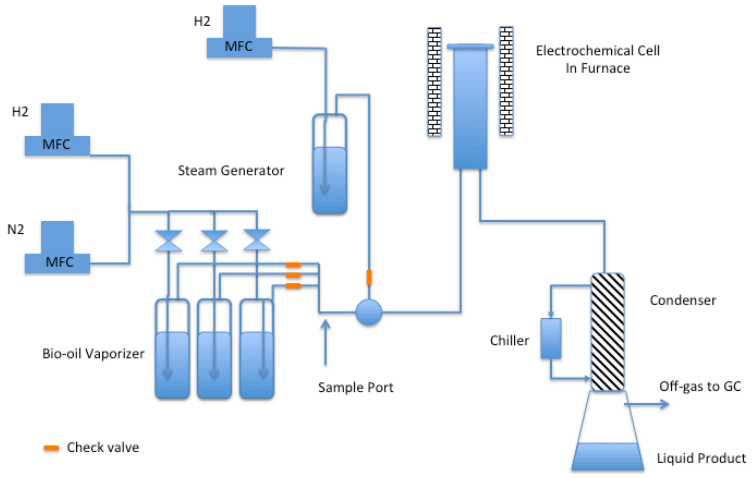

Figure 7. Schematic of EDOx Test Rig

Because of the difficulty in feeding mixtures of model compounds later experimental set up used either a syringe pump or a controlled evaporative mixer.

Model Compound Electrolysis Tests

Test Validation

A series of electrolysis tests were performed using different model compounds. The objective of the initial test to prove that no external hydrogen is needed during cell operation. Cell 14ULT_27 using zirconia electrolyte was initially operated on steam with H_2 and N_2 flowing at 30 sccm each through an 82 °C heated water bubbler. An additional feed acetic acid vapor from an 82 °C heated bubbler with N_2 as the carrier gas at 30 sccm of flow. After 15 minutes the H_2 in the steam bubbler was turned off and the N_2 was doubled to maintain the same steam flow rate. The cell was operated for 105 min where no external hydrogen was provided. As can be seen in Figure 8, the cell performance was very stable. The Acetic Acid flow was then turned off and the standard conditions for the water bubbler were returned. The current density response at a constant voltage of 1.3V can be seen below for each of these conditions. This test clearly showed that during EDOx cell operation no external hydrogen need to be provided.

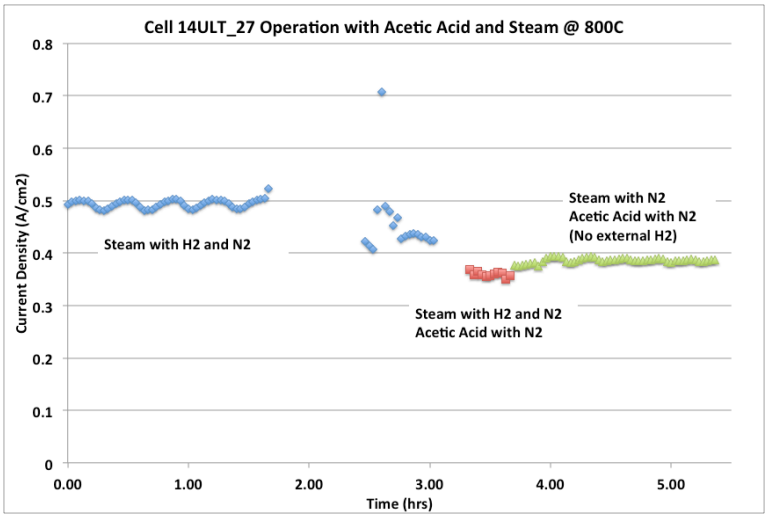

Figure 8. Model Compound (Acetic Acid) Test

Acetic Acid and Acetone

Cell # 14ULT_28 was tested at 700 °C using acetic acid and steam with N_2 as the carrier gas. The two streams were fed from separate heated containers and the resulting vapors were mixed prior to entry into the fuel manifold of the cell. This was tested at three different current densities as well as at the open circuit condition (OCV). There is no current through the cell under OCV conditions. Hydrogen was added to the steam in the OCV condition to prevent oxidation of the fuel electrode. Under an applied voltage, hydrogen is generated in situ by the electrolysis of steam. The exhaust product gas was analyzed using a micro-GC for each condition. This cell was also tested on acetone with N_2 as the carrier gas and with steam and N_2 at both 700 °C and 800 °C test temperatures. Three different current densities were tested at each temperature and GC samples were analyzed for each. The gas composition results from the GC sampling for each test condition are given below in Table *4*.

From Table *4*, it can be seen that at no current condition, the external hydrogen favors formation of some product catalyzed by the electrode material. Under current producing condition, hydrogen production occurs from the electrolyzed steam and that it is more favored using acetone over acetic acid. Also using acetone at 800 °C produces more CH_4 and CO with less butane than is produced at 700 °C.

In order to reduce the cell operating temperature to one that is more in line with the bio-oil reactor temperature, cells made from ceria electrolyte were tested. A ceria electrolyte cell #14SDC_30 was tested on furfural at 550 °C using two different current density values and at OCV. The furfural was vaporized at a temperature of 50 °C with N_2 flowing and the steam had only N_2 as the carrier gas except for the OCV condition, which also had additional H_2. Table *5* contains the GC results for the gas product at different current density values and at OCV. As before at OCV, external hydrogen was provided.

Table 4. Product gas analysis from cell # 14ULT_28 on acetic acid and acetone.

Temp	Organic	Voltage	Current	H2	CH4	CO	CO2	Ethene	Ethane	Propane	Butane
700	Acetic Acid	1.300	0.113	39.4%	1.8%	34.0%	5.9%			18.3%	
700	Acetic Acid	1.115	0.082	36.9%	1.4%	39.1%	5.7%			16.2%	
700	Acetic Acid	0.973	0.050	35.5%	1.5%	40.1%	5.8%			16.4%	
700	Acetic Acid	0.828	0.000	65.9%	1.2%	22.2%	2.9%			7.6%	
700	Acetone	1.300	0.046	79.5%	3.0%	7.1%	0.4%	0.2%	0.2%	0.7%	9.0%
700	Acetone	1.450	0.080	70.6%	9.0%	6.0%	0.8%	0.2%	0.2%	0.7%	12.4%
700	Acetone	1.600	0.116	70.1%	9.1%	6.1%	0.8%	0.2%	0.2%	0.8%	12.8%
800	Acetone	1.300	0.175	48.4%	27.4%	19.3%	0.9%	0.6%	0.6%	0.9%	0.7%
800	Acetone	1.450	0.244	46.5%	28.8%	19.7%	0.6%	0.7%	0.7%	0.8%	0.8%
800	Acetone	1.600	0.331	43.1%	30.9%	20.9%	0.7%	1.0%	1.0%	1.0%	

Table 5. Product gas analysis from cell # 14SDC_30 on furfural.

Temp	Organic	Voltage	Current	H2	CH4	CO	CO2	Ethene	Ethane	Acetylene	Propane	Butane	Pentane
550	Furfural	1.30	0.06	3.0%		20.1%	35.3%	0.8%		1.2%	36.6%		3.1%
550	Furfural	1.60	0.10	1.8%		18.1%	34.5%	1.0%		1.0%	40.9%		2.8%
550	Furfural	0.76	0.00	96.7%		0.3%	0.1%				2.9%		

Guaiacol, Furfural, Phenol, Syringol

Cell #14SDC_31 was another ceria electrolyte cell that was tested at 550 °C using several different organics. It was independently tested on guaiacol, furfural, phenol, and syringol. The cell was tested at different current densities for each material except for furfural and syringol where it was tested at one condition to generate some condensate for GCMS testing. All other materials were also left on test at one current density long enough to generate condensate for analysis. Nitrogen was used as the carrier gas for each chemical and N2 with H2 was used as a carrier gas for the steam, but at a reduced flow rate. The water temperature was lowered to 50 °C from the 82 °C used in previous cells to reduce the amount of available water to electrolyze. Table *6* contains the gas phase GC results for each condition.

Table 6.Output gas compositions using model compounds

Temp	Organic	Voltage	Current	H2	CH4	CO	CO2	Ethene	Ethane	Propane	Butane	Pentane
550	Guaiacol	1.3	0.24	85.3%	2.7%	5.4%	1.9%	0.3%	0.1%	4.0%	0.2%	0.1%
550	Guaiacol	1.39	0.36	85.1%	2.9%	5.4%	1.8%	0.3%	0.2%	3.9%	0.3%	0.1%
550	Guaiacol	0.845	0	80.2%	3.7%	7.3%	3.8%	0.3%	0.2%	3.9%	0.4%	0.1%
550	Guaiacol	1.55	0.748	83.0%	3.3%	6.3%	1.8%	0.3%	0.2%	4.6%	0.3%	0.1%
550	Furfural	1.38	0.36	89.9%		3.7%	2.2%	0.1%		3.9%		0.2%
550	Furfural	1.35	0.341	91.3%		2.4%	2.3%	0.1%		2.5%		1.4%
550	Phenol	1.35	0.43	96.8%		0.9%	0.5%			1.9%		
550	Phenol	0.742	0	85.7%		1.6%	5.6%			7.1%		
550	Phenol	1.4	0.351	88.3%		1.7%	4.8%			5.2%		
550	Phenol	1.15	0.092	88.0%		1.7%	5.0%			5.3%		
550	Phenol	1.6	0.757	86.4%		1.6%	5.5%			6.4%		
550	Syringol	1.63	0.33	73.3%	1.7%	3.9%	12.3%	0.4%		8.3%	0.2%	
550	Syringol	1.69	0.142	71.3%	2.1%	5.0%	12.2%	0.3%	0.1%	8.7%	0.2%	

These materials all produced CO, CO_2 and propane in the gas phase products. The guaiacol and syringol were similar and also produced methane, ethane, ethane, and butane. The guaiacol did produce some pentane. The phenol only produced the CO, CO_2, and propane, while the furfural also produced ethane and pentane.

A liquid condensate sample from each of these tests was collected and only the guaiacol condensate has been extracted and analyzed using the GCMS. The condensate separated into two distinct layers.

Analysis of liquid product from Guaiacol feed

A feed rate of 1.67 g/hr of guaiacol was vaporized using undiluted compound. Additional feed to the included 10 sccm of H_2, 30 sccm of N_2, and 6.6 sccm of steam. At the peak electric current conditions, 30% of oxygen from the feed was removed. This condition was chosen in order to avoid possibility of coking on the electrode so that sufficient product can be collected for analysis. The pure guaiacol and product collected from the EDOx cell are shown in Figure *9*.

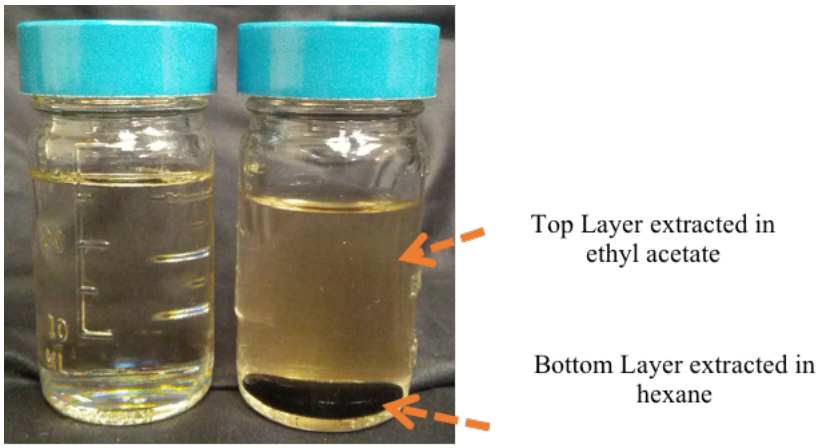

Figure 9. Pure guaiacol (left) and EDox product (right)

The product separated into two separate phases. The darker phase at the bottom was extracted using hexane and the top lighter solution was extracted into ethyl acetate for Gas Chromatograph / Mass Spectrometer (GC-MS) analysis. Blank solutions of hexane and ethyl acetate were run to ensure that no contaminants were present in the extraction solution. The results from the analysis of the top and bottom layers are shown in Figure 10.

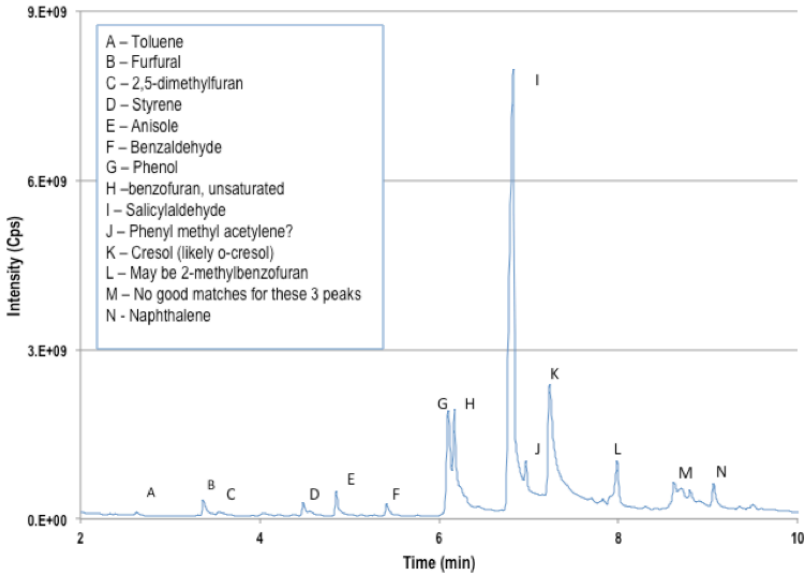

a. Top Layer components (extracted in ethyl acetate)

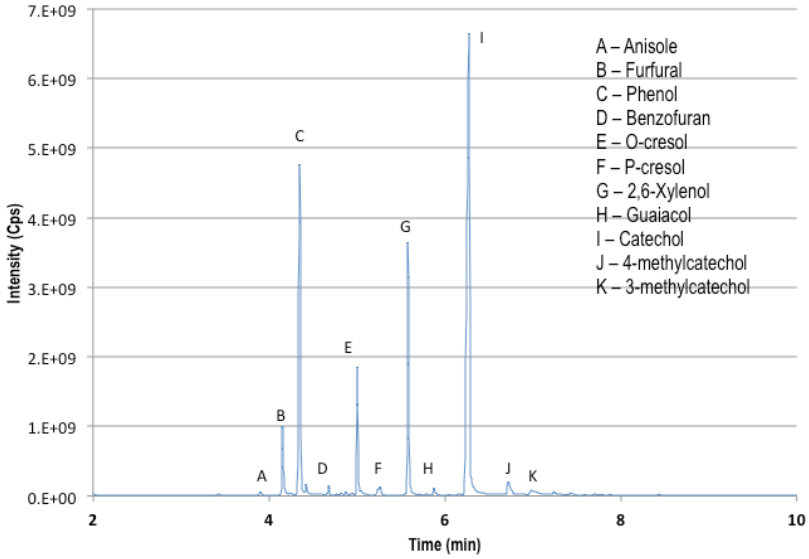

b. Bottom layer components (extracted in hexane)

Figure 10. GC-MS Analysis Results of EDox Product Liquid with Guaiacol Feed

The molecular structure of the feed guaiacol and the various products are shown in Figure 11. As can be seen, more than 20 identifiable products were collected. In addition to complex rearrangement of structure with the removal of oxygen, several compounds have one or no oxygen compared to guaiacol which has two oxygen, a phenolic and methoxy functional groups. It is quite likely that part of the product suite may be dependent upon the catalytic properties of the electrode material. All tests were performed using fuel electrode compositions that are routinely used for steam and steam + carbon dioxide electrolysis cells.

In summary, several simple compounds (acetone and acetic acid) and bio-oil model compounds (guaiacol, furfural, phenol, and syringol) were tested separately using EDox cells for deoxygenation properties. In all cases a variety of deoxygenated hydrocarbon gases (methane, ethane, ethane, propane,

butane, pentene) as well numerous liquid phase hydrocarbons were produced. Liquid product from guaiacol was extensively analyzed and was found to contain more than 20 species with several of them partially or fully deoxygenated. Some of the compounds were a complex rearrangement of guaiacol radicals. It is expected that catalytic modification to the electrode may prove to be useful in increasing the selectivity of specific product distribution.

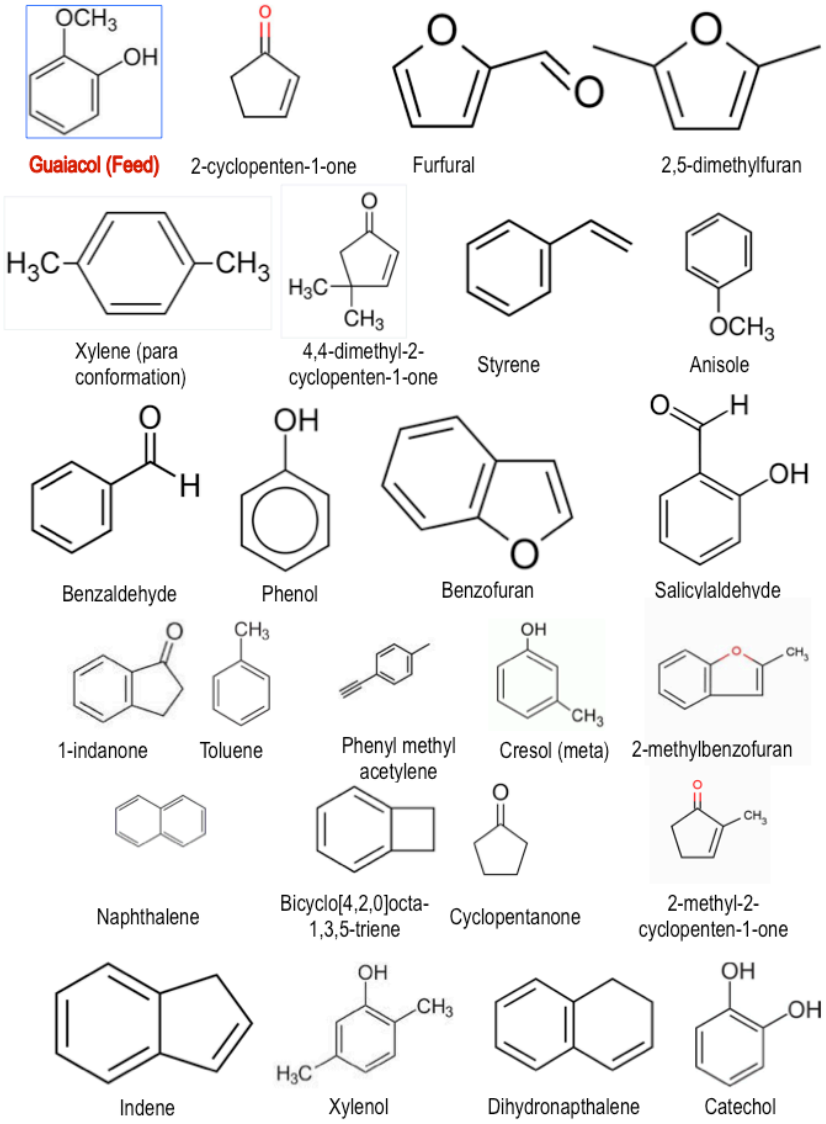

Figure 11. Products of electrolysis of guaiacol

Based on the promising results of this cell, additional button cells were tested using a low temperature electrolyte at 550 °C.

Ceria Button Cell Syringol

For cell #32**,** a ceria electrolyte was installed into a cleaned and sealed test rig. The current collectors were Ni on the fuel side and Ag on the airside. A reservoir containing syringol was heated to 50 °C with 30 sccm of N_2 flowing through the compound to carry the saturated vapor. Steam was generated in a water bubbler that was heated to 80 °C. A 15 sccm of N_2 was used as the carrier gas for steam. The two streams were mixed prior to entering the fuel manifold of the button cell. The liquid product from the syringol run

from the electrochemical cell was collected in a container chilled to about 10 – 12 °C, and analyzed using GC-MS to determine the product composition. *Table 7* gives the product comparison to the feed stream, showing a complete conversion of the syringol to products with reduced oxygen content. No syringol was detected in the collected liquid product.

Table 7.*Syringol Feed and Liquid Product Composition Comparison for Cell 32*

Feed

Compound	**C**	**H**	**O**
Syringol	8	10	3

Liquid Product

Compound	**C**	**H**	**O**	**wt %**
Phenol	6	6	1	76%
o-cresol	7	8	1	22%
p-cresol	7	8	1	0%
m-cresol	7	8	1	0%
2,6-xylenol	8	10	1	1%
2-ethylphenol	8	10	1	1%

Table 8 provides the overall elemental balance between the syringol feed and the end liquid product. The balance shows a 47.2% reduction in the oxygen weight percent of the feed and the liquid products. Based on this test, it appears that Syringol has a theoretical maximum oxygen reduction of 66% (on the basis of number of oxygen atoms per molecule) with the end product being a phenol-like compound. Interesting to note is that fact that there is a net increase in carbon and hydrogen weight fraction indicative of high C and H efficiency for the process.

Table 8. Elemental Balance between Syringol Feed and Liquid Product on Cell 32

Element	**Feed wt% By Formula**	**Liquid Product wt% by GC**	**Feed to Product % Change**
Carbon	62.3%	76.9%	23.3%
Hydrogen	6.5%	6.7%	2.3%
Oxygen	31.1%	16.4%	**-47.2%**

Table 9 does not include the overall system balance. The results from the GC analysis of the gas product from the Syringol button cell run are shown in Table 3. As can be seen in these results, there are additional deoxygenated products in the gas stream, as well as products of the electrolyzed steam feed. The inclusion of this analysis will improve, in effect, the reduction of the overall weight percent oxygen, as well as increase the total carbon retention.

Table 9. Gas Product Micro-GC Analysis for Syringol on Cell 32

Component	H_2	N_2	Methane	CO	CO_2	Ethene	Ethane	Propane
wt%	0.01%	93.7%	0.1%	0.9%	3.8%	0.1%	0.1%	1.4%

Ceria Button Cell Guaiacol

Cell #35 was constructed the same as cell #32 but was from a new batch. The current collectors were Pt on both the fuel side and the airside. The cell was heated in H_2 to reduce the fuel electrode from NiO-ceria state to Ni-ceria state, and was then cooled before. Guaiacol and steam were fed from independent heated reserovirs and the performance monitored at a cell voltage of 1.3 V. A GC sample was taken during

the guaiacol feed (9 sccm N_2, water with 7 sccm N_2). The cell voltage was then increased from 1.3 to 1.8 V and the same feed conditions applied. After the voltage increase, another sample was collected.

A comparison of the liquid products for each voltage condition is given in *Table 10*. The variance in product selectivity is believed to be due to interaction of the feed stream with the electrode under the given conditions, but the mechanism is still being investigated. As can be seen, most of the liquid products that were identified had 2 oxygens (no net reduction/molecule, but major molecular rearrangement) or 1 oxygen (50% oxygen reduction on a molecular basis), or no oxygen (100% reduction). However, the selectivity appears to be high for phenolic (1 oxygen) compounds. Additionally, higher voltage operation produced more compounds in the product with some of them with no oxygen.

Table 10. Guaiacol Feed and Liquid Product Composition Comparison for Cell 35 at 1.8 and 1.3 V

Feed

Compound	**C**	**H**	**O**
Guaiacol	8	10	3

Liquid Product 1.8 V

Compound	**C**	**H**	**O**	**wt %**
Unknown C6H8O	6	8	1	0.40
Anisole	7	8	1	0.08
Cyclopentanone	5	8	1	0.02
2-cyclopenten-1-one	5	6	1	0.09
Phenol	6	6	1	27.83
2-methyl-2-cyclopenten-1-one	6	8	1	0.47
Benzaldehyde	7	6	1	0.87
4,4-dimethyl-2-cyclopenten-1-one	7	10	1	0.40
o-cresol	7	8	1	7.76
p-cresol	7	8	1	1.05
m-cresol	7	8	1	0.89
Salicylaldehyde	7	6	2	7.91
2,5-xylenol	8	10	1	0.24
2-ethylphenol	8	10	1	4.16
Guaiacol-like molecule	7	8	2	0.66
3-Methylbenzaldehyde	8	8	1	0.14
3-Methyl-2-cyclopenten-1-one	6	8	1	0.04
2-Methylbenzofuran	9	8	1	0.23
Naphthalene	10	8	0	0.14
Catechol	6	6	2	42.24

Liquid Product 1.3 V

Compound	**C**	**H**	**O**	**wt %**
2,3-dihydrofuran	4	6	1	0.14
Unknown C6H8O	6	8	1	1.54
2-cyclopenten-1-one	5	6	1	0.68
Phenol	6	6	1	48.76
2-methyl-2-cyclopenten-1-one	6	8	1	0.51
Benzaldehyde	7	6	1	0.93
4,4-dimethyl-2-cyclopenten-1-one	7	10	1	0.56
o-cresol	7	8	1	18.02
Salicylaldehyde	7	6	2	28.47
2,5-xylenol	8	10	1	0.39

3-methylcatechol	7	8	2	0.94
4-methylcatechol	7	8	2	0.65
2-Methylnapthalene	11	10	0	0.16
1H-indenol	9	8	1	1.93
1-Indanone	9	8	1	0.11
Cinnamaldehyde	9	8	1	0.47
Acenapthylene	12	8	0	0.07
Dibenzofuran	12	8	1	0.04

Table 11 provides the elemental balance between the guaiacol feed and the collected liquid products at each voltage condition. Guaiacol appears to have a maximum theoretical oxygen reduction potential of 50% (on a number of oxygen per molecule basis), with high selectivity for a phenol-type compound for the electrocatalyst that was used. There is 13% and 25% reduction in the wt% of oxygen in the product relative to the feed model compound.

Table 11.*Elemental Balance between Guaiacol Feed and Liquid Product on Cell 35 at 1.8 V and 1.3 V*

		Cell 35 1.8 V		**Cell 35 1.3 V**	
Element	**Feed wt% by Formula**	**Liquid Product wt% by GC**	**Feed to Product % Change**	**Liquid Product wt% by GC**	**Feed to Product % Change**
Carbon	67.7%	71.5%	5.6%	74.55%	10.1%
Hydrogen	6.5%	6.1%	-6.0%	-6.26%	-3.7%
Oxygen	25.8%	22.4%	**-13.1%**	19.19%	**-25.5%**

Again, the system does not currently account for the gas product in the overall elemental balance. The gas product composition was quantified using GC and these results are available in *Table 12*.

Table 12.*: Gas Product Micro-GC Analysis for Guaiacol on Cell 35 at 1.8 V and 1.3 V*

Component	H_2	N_2	CH_4	CO	CO_2	Ethene	Ethane	Propane	Butane	Pentane
wt % 1.3 V	0.05%	95.7%	0.17%	0.00%	2.27%	0.04%	0.06%	1.71%	0.01%	0.02%
wt % 1.8 V	0.21%	94.0%	0.69%	0.00%	4.07%	0.01%	0.02%	1.64%	0.00%	0.00%

Initial Stack Testing

Guaiacol – Stack 541

Stack 541 is a standard electrolysis stack with ScSZ-doped zirconia electrolyte and a 45 cm^2 electrode active area. The stack was heated to 800 °C and tested in electrolysis mode with a water bubbler maintained at 85 °C, and 0.8 slpm flows each (verify) through the bubbler for the N_2 and H_2. as the steam carrier gasAt the selected water bubbler temperature, the steam content of the carrier gas is calculated to be 50%. The test at 800 °C was performed to benchmark stack performance. A stack current of 15 A was achieved at a voltage of 7.8 V (1.3 V/cell) which is typical of such stack materials and configuration. The stack was then cooled to 550 °C for model compound testing. Guaiacol was filled into organic second reservoir. At the selected reservoir temperature, the vapor fraction of guaiacol in the carrier was ~25%. The steam was shut off and the stack was allowed to stabilize. With no steam flowing, the stack only received guaiacol vapor as the feed.

The GC-MS of the liquid product showed an interesting set of components in comparison with the guaiacol on the button cell (*Table 13*). Though at very low concentrations, this was the first product collection where multiple components with zero oxygen groups were detected. This demonstrates that a pathway is present to deoxygenate past the phenol compound by improved selectivity to the less oxygenated compounds.

Table 13.: *Guaiacol Feed and Liquid Product Composition Comparison for Stack 541*

Feed

Compound	C	H	O
Guaiacol	8	10	3

Liquid Product

Compound	C	H	O	wt %
Toluene	7	8	0	0.04%
Styrene	8	8	0	0.05%
Anisole	7	8	1	0.43%
1,2,4-Trimethylbenzene	9	12	0	0.34%
2-cyclopenten-1-one	5	6	1	0.20%
Phenol	6	6	1	11.07%
Methyl Anisole	8	10	1	0.13%
Benzofuran	8	6	1	0.85%
2-methyl-2-cyclopenten-1-one	6	8	1	0.25%
Benzaldehyde	7	6	1	0.13%
o-cresol	7	8	1	8.71%
p-cresol	7	8	1	0.57%
m-cresol	7	8	1	0.30%
Salicylaldehyde	7	6	2	20.65%
2,6-xylenol	8	10	1	0.22%
2-ethylphenol	8	0	1	4.96%
Guaiacol	7	8	2	2.47%
2,3-dihydrobenzofuran	8	8	1	0.66%
Naphthalene	10	8	0	0.57%
1,2-dimethoxybenzene	8	10	2	1.89%
Catechol	6	6	2	39.81%
3-methylcatechol	7	8	2	2.78%
4-methylcatechol	7	8	2	2.22%
α-cedrene?	15	24	0	0.10%
o-anisaldehyde	8	8	2	0.07%
2,3-dihydro-1H-inden-1-one	9	8	1	0.17%
Benzalmalonic dialdehyde?	10	8	2	0.04%
o-bidiphenylol?	10	12	1	0.05%
Dibenzofuran	12	8	1	0.15%
4-ethyl-3-methylphenol	9	12	1	0.04%
2-methylbenzofuran	9	8	1	0.07%

Table 14 provides the elemental balance between the guaiacol feed and the collected liquid product at each voltage condition. Though the oxygen reduction level is lower in this stack test than it was in the Cell 35 test, the presence of the oxygen free compounds is promising especially since the selectivity for these can be improved by optimizing the operating parameters of the system.

Table 14. *Elemental Balance between Guaiacol Feed and Liquid Product on Stack 541*

Element	**Feed wt% by Formula**	**Liquid Product wt% by GC**	**Feed to Product % Change**
Carbon	67.7%	70.58%	4.2%
Hydrogen	6.5%	5.57%	-14.2%
Oxygen	25.8%	23.85%	**-7.5%**

The gas product analysis, shown in *Table 15*, also shows completely deoxygenated compounds, which once incorporated into the system's mass balance will decrease the oxygen content of the product stream.

Table 15: Gas Product Micro-GC Analysis for Guaiacol on Stack 441

Component	H_2	N_2	CH_4	CO	CO_2	Ethene	Ethane	Propane	Butane	Pentane
Wt %	0.05%	95.3%	0.18%	0.00%	2.46%	0.05%	0.07%	1.85%	0.01%	0.02%

Aqueous Phase Bio Oil Testing – Button Cell

A sample of the pyrolysis oil aqueous phase (140321 Yellow Pine-Aqueous Phase) was provided to Ceramatec by PNNL for testing. The initial characterization performed by PNNL is included Table 16 *and*

Table 17. This analysis done was on a wet-basis. GC-MS analysis on 140321 Yellow Pine-Aqueous phase is shown in Table 10 with peak identification based on at least 80% of match to library compounds, these peaks represents at least 50% of the total chromatogram peak area.

Table 16. GC Analysis of Yellow Pine-Aqueous Phase (Bio Oil) Sample from PNNL

Component	**Total area distribution**
Levoglucosan and other anhydrosugar isomers	25.9%
Acetic acid	4.8%
benzenediol (catechol)	4.6%
hydroxyacetone	3.1%
hydroxymethoxyphenylpropanone(acetone-guaiacol)	2.5%
methyl catechol	1.5%
furfural	1.3%
ethanone-guaiacol (vanilin)	1.3%
propyl-guaiacol	1.1%
propanoic acid	0.8%
furanone	0.8%
hydroxybutanone	0.8%
hydroxymethylcyclopentenone (corylone)	0.8%
methoxy-phenol (guaiacol)	0.7%
phenol	0.6%
methyl-guaiacol	0.6%
cyclopentanone	0.6%
methyl phenol	0.5%
Other	47.7%

Table 17. *CHNS Analysis of Yellow Pine-Aqueous Phase (Bio Oil) Sample from PNNL*

	ASTM D5379/D5291			ASTM D4239/D1552	
	C	**H**	**N**	**S**	**O (by diff)**
140321 Yellow Pine-Aqueous	21.11%	9.00%	0.01%	<0.01%	69.9%
duplicate	21.21%	8.99%	0.01%	<0.01%	69.8%
average	21.16%	8.995%	0.01%	<0.01%	69.8%

These numbers were on a wet basis. Karl Fisher titration was also done by PNNL on 140321 Yellow Pine-Aqueous determining the water content to be 58.645±0.631 wt%.

With the bio-oil containing multitude of compounds, feed composition was first determined by evaporating it at 90 °C and analyzing the condensate. An extraction method using ethyl acetate was utilized to avoid injection water onto the GC-MS column, thus providing a dry basis. *Table 18* shows the representative composition of the feed stream used for all bio oil testing.

Table 18. *90 °C Bio Oil Condensate Composition Analysis by GC-MS*

Compound	C	H	O	wt %
Acetic Acid	2	4	2	11.34%
2-methoxytetrahydrofuran	5	10	2	0.09%
2,3-butanedione	4	6	2	0.48%
2-Butenal	4	6	1	0.28%
Hydroxyacetone	3	6	2	16.14%
Acetoin	4	8	2	2.42%
3-penten-2-one	5	8	1	1.44%
1-hydroxy-2-butanone	4	8	2	6.02%
Cyclopentanone	5	8	1	1.76%
3-Furaldehyde	5	4	2	0.86%
2-Butoxyethanol	6	14	2	4.36%
Furfural	5	4	2	9.85%
2-cyclopenten-1-one	5	6	1	13.82%
Phenol	6	6	1	3.07%
2-methyl-2-cyclopenten-1-one	6	8	1	4.64%
Acetylfuran	6	6	2	1.05%
2,3-dimethyl-2-cyclopenten-1-one	7	10	1	0.18%
o-cresol	7	8	1	2.64%
Acetol acetate	5	8	3	2.62%
p-cresol	7	8	1	0.40%
m-cresol	7	8	1	0.48%
5-methyl-2-furancarboxaldehyde	6	6	2	1.57%
5-methylfurfural	6	6	2	1.57%
Xylenol	8	10	1	0.03%
3-methyl-1,2-cyclopentadione	6	8	2	0.66%

Unknown C6H8O	6	8	1	1.90%
Unknown C7H10O	7	10	1	0.89%
1-(acetyloxy)-2-butanone	6	10	3	0.40%
Guaiacol	7	8	2	6.19%
5-methyl-2(5H)-Furanone	5	6	2	0.54%
2,5-dihydro-3,5-dimethyl-2-furanone	6	8	2	0.64%
3-ethyl-2-cyclopenten-1-one	7	10	1	0.16%
Creosol	8	10	2	1.48%

Testing Conditions and Results – Ceria Button Cell

Button Cell – Cell 39

Cell 39 using a ceria (Sm doped ceria – SDC) electrolyte was constructed the same as Cell 32. The current collectors were Pt on the fuel side and Pt on the airside. The cell was heated to 750 °C to reduce the fuel electrode (OCV was 0.76V) and then cooled to 550 °C. The cell was operated at 1.3 V with an average current of around 0.17 A.

With this complex feed stream, it is interesting to note the comparison of compound types found in the liquid product stream. As can be seen in *Table 19*, there were multiple products not originally present in the feed. There are also compounds missing in the product stream, showing that these compounds were entirely converted to different compounds.

Table 19. *Bio Oil Feed and Liquid Product Composition Comparison for Cell 39*

Compound	**C**	**H**	**O**	**Bio Oil Feed (90 °C reference feed) wt %**	**Cell 39 Liquid wt %**
2,3-dihydrofuran	4	6	1		3.12%
Acetic Acid	2	4	2	11.34%	
2-methoxytetrahydrofuran	5	10	2	0.09%	
2,3-butanedione	4	6	2	0.48%	
2-Butenal	4	6	1	0.28%	
Hydroxyacetone	3	6	2	16.14%	19.48%
Acetoin	4	8	2	2.42%	2.20%
3-penten-2-one	5	8	1	1.44%	2.21%
1-hydroxy-2-butanone	4	8	2	6.02%	
Cyclopentanone	5	8	1	1.76%	7.28%
3-Furaldehyde	5	4	2	0.86%	1.93%
2-Butoxyethanol	6	14	2	4.36%	
Furfural	5	4	2	9.85%	24.20%
2-cyclopenten-1-one	5	6	1	13.82%	18.58%
Phenol	6	6	1	3.07%	3.41%
2-methyl-2-cyclopenten-1-one	6	8	1	4.64%	10.86%
Acetylfuran	6	6	2	1.05%	1.82%
2,3-dimethyl-2-cyclopenten-1-one	7	10	1	0.18%	
o-cresol	7	8	1	2.64%	

Acetol acetate	5	8	3	2.62%	2.21%
p-cresol	7	8	1	0.40%	
m-cresol	7	8	1	0.48%	
5-methyl-2-furancarboxaldehyde	6	6	2	1.57%	1.96%
5-methylfurfural	6	6	2	1.57%	
Xylenol	8	10	1	0.03%	
3-methyl-1,2-cyclopentadione	6	8	2	0.66%	
Unknown C6H8O	6	8	1	1.90%	
Unknown C7H10O	7	10	1	0.89%	
1-(acetyloxy)-2-butanone	6	10	3	0.40%	
Guaiacol	7	8	2	6.19%	
2,3-dimethyl-2-cyclopenten-1-one	7	10	1		0.73%
5-methyl-2(5H)-Furanone	5	6	2	0.54%	
2,5-dihydro-3,5-dimethyl-2-furanone	6	8	2	0.64%	
3-ethyl-2-cyclopenten-1-one	7	10	1	0.16%	
Creosol	8	10	2	1.48%	

An elemental balance between the 90 °C condensate and the liquid product collected from the Cell 39 run is provided in *Table 20*. The overall reduction of oxygen from the feed to the product was 24.6%, which, as previously discussed, does not include the balance from the gas product stream(*Table 21*).

Table 20. Elemental Balance between Bio Oil Feed and Liquid Product on Cell 39

Element	**Feed Wt% by GC-MS**	**Liquid Product Wt% by GC-MS**	**Feed to Product % Change**
Carbon	60.93%	70.58%	15.8%
Hydrogen	7.42%	5.57%	-24.9%
Oxygen	31.65%	23.85%	**-24.6%**

Table 21. Gas Product Micro-GC Analysis for Bio Oil on Cell 39

Component	H_2	N_2	CH_4	CO	CO_2	Ethene	Ethane	Propane	Butane
Wt %	0.40%	92.95%	0.15%	2.17%	2.02%	0.09%	0.02%	2.17%	0.02%

Zirconia Button Cell Testing

In order to compare the performance of zirconia electrolyte based button cells against the performance of ceria electrolyte based button cells, additional testing was performed using syringol as the model compound with zirconia based button cells.

Syringol Liquid Product Comparison Via GC-MS

Two types of tests were one performed. In the first test (#1411-1), a 2-cm^2 active electrode area zirconia cell was tested 550 °C under no current condition. 4 sccm of hydrogen was fed along with 0.0189g/hr syringol vapor and 0.287g/hr steam. The analysis of the liquid product collected shows that nearly 50% of the oxygen from syringol was removed, although without an electric current the removed oxygen would have stayed on the same side as the feed model compound and likely reacted **w**ith the hydrocarbon vapors.

However, the test clearly shows the effectiveness of the electrode material to function as deoxygenation catalyst.

In a second test (#1502-1), the syringol vapor and steam were fed to the cell without feeding any hydrogen along with it. The cell was operated at 1.6 V. Analysis of collected liquid product showed similar amount of deoxygenation (44%) as with no current. It should be noted however that no hydrogen was fed with the model compound and any hydrogen that participated in the deoxygenation process was electrochemically produced from the electrolysis of steam. Interestingly, the extent of deoxygenation using the zirconia cell is nearly identical to the earlier ceria cell that was tested. The results are tabulated in Table 22. The GC-MS analysis results from the liquid product is also given. In all cases (ceria under current, zirconia under no current and current) showed the product is largely phenol and cresol (going from 3 oxygen syringol to 1 oxygen product). However, additional products were observed (e.g. xylenol and ethyl phenol) with electrical current through the cell indicating that the electrolysis operation results in additional molecular rearrangement over fully catalytic, no current condition.

Table 22. Button cell test results using Syringol

Syringol SOEC, 1411-1, Zirconia, 2cm^2, 550C, OCV, 4 sccm H2				
Element	**Feed wt frac. By Formula**	**Liquid Product wt frac. by GC**	**Water Feed Composition wt %**	**Feed to Product % Change**
Carbon	0.623	0.773	93.820	24.08%
Hydrogen	0.065	0.070		8.53%
Oxygen	0.311	0.157		**-49.61%**

Syringol SOEC, 1502-1, Zirconia, 2cm^2, 550C, 1.6V				
Element	**Feed wt frac. By Formula**	**Liquid Product wt frac. by GC**	**Water Feed Composition wt %**	**Feed to Product % Change**
Carbon	0.623	0.758	approx. 94	21.68%
Hydrogen	0.065	0.070		7.16%
Oxygen	0.311	0.173		**-44.51%**

Q4 Syringol SOEC, Cell 32 Ceria 1.5cm^2, 1.3V				
Element	**Feed wt frac. By Formula**	**Liquid Product wt frac. by GC**	**Water Feed Composition wt %**	**Feed to Product % Change**
Carbon	0.623	0.769	Not determined	23.49%
Hydrogen	0.065	0.067		3.29%
Oxygen	0.311	0.164		**-47.33%**

LIQUID PRODUCT GC-MS						
Compound	**C**	**H**	**O**	**Cell 32 wt %**	**Cell 1502-1 wt %**	**Cell 1411-1 OCV wt %**
Phenol	6	6	1	76	29	40.4
o-Cresol	7	8	1	22	39	59.6
p-Cresol	7	8	1	0	0.42	0
m-Cresol	7	8	1	0	2.7	0
2,6-Xylenol	8	10	1	1	0	0
2,3-Xylenol	8	10	1	0	1.5	0
2-Ethylphenol	8	10	1	1	9.9	0

Syringol

Test was conducted using syringol and water mixture using a button cell at 550 °C. Because of low current density in prior tests, this test was done at a higher voltage of 1.8 V and an average current of 198 mA was maintained. A schematic and summary of results are shown in Figure 12. For clarity the liquid product analysis is also shown in a separate table. Post-test visual inspection of the cell, as mentioned earlier, showed reduced zirconia which may have affected current efficiency of this test. Nonetheless, the results clearly showed removal of two oxygen atoms from the syringol molecule to produce largely phenol as the liquid product. Note that analysis of syringol-water evaporated at 190 °C retained the syringol without decomposition. The gas analysis is shown in

Table 23.

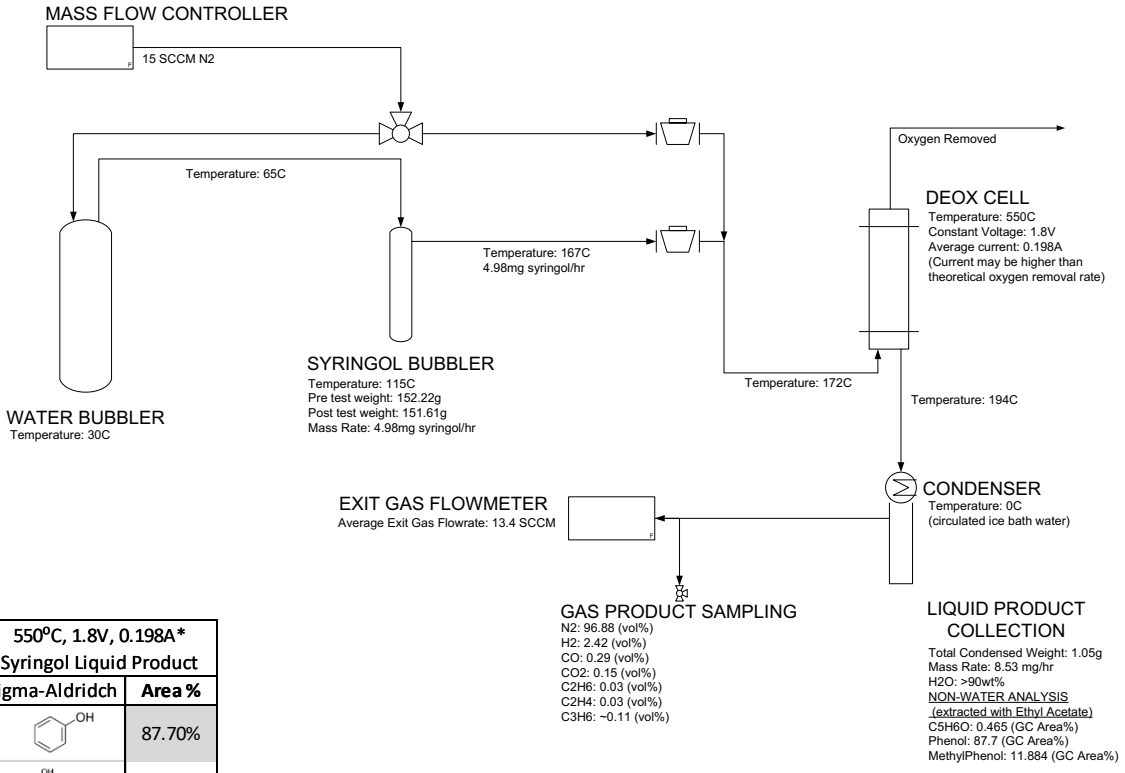

550°C, 1.8V, 0.198A* Syringol Liquid Product	
Sigma-Aldridch	**Area %**
	87.70%
	11.84%
C5H6O	0.46%

Figure 12. Schematic of Syringol Test System

Table 23. Gas Product Analysis of Syringol Test

1.8V Syringol, Product Gas Analysis	
Compound	**Mass % (no N_2, O_2)**
Hydrogen	18.63%
Carbon Monoxide	31.63%
Carbon Dioxide	24.67%
Ethane	3.60%
Ethene	2.72%
Propane	18.75%

Mixture of Model Compounds

Syringe pump provides a more accurate feed mechanism compared to a heated bubbler bath. If a mixture of model compounds were to be fed to the cell, use of a heated bubbler would provide time varying composition depending on the vapor pressure of each of the compound in the mixture. A syringe pump, which feeds the liquid mixture to be evaporated a more consistent composition can be fed. Bio-oil vapor is a more complicated mix of compounds to simulate and we chose a simple four compound mixture that will stay as a single liquid without phase separation. The selected mixture contained an alcohol, ketone, acid and water as shown in the left section of Table 24.

The model compound mixture was fed to a hot zone consisting of manifolded blank zirconia electrolyte without any electrode. The center section of the table provides the analysis of the collected output liquid from the test. The 2,4-dimethylpentanone is largely intact showing 63% in the collected sample. A small amount of 2-methyl-2-cyclopenten-1-one was also observed. It appears that both syringol and acetic acid thermally decomposed. Several phenolic compounds were also seen in minor quantities.

The last section of the table shows the product liquid composition after a button cell test operated at 550 °C. The cell voltage was maintained at 1.5 V to avoid reduction of zirconia and the current stabilized at about 5 mA. Significant reduction in the amount of 2,4-dimethylpentanone was seen. Other major compounds include methyl phenol (slightly more than thermal decomposition product), catechol, ethyl phenol, and phenol and minor amounts of other phenolic compounds. Liquid compounds above 1% area are included. All gas sample mass percents were calculated on Molecular weight basis, from GC tabulated area percentages. The gas data in Table 25 represent the Micro GC analysis of product gases.

A schematic of the process flow for the 4-model compound mixture is shown below.

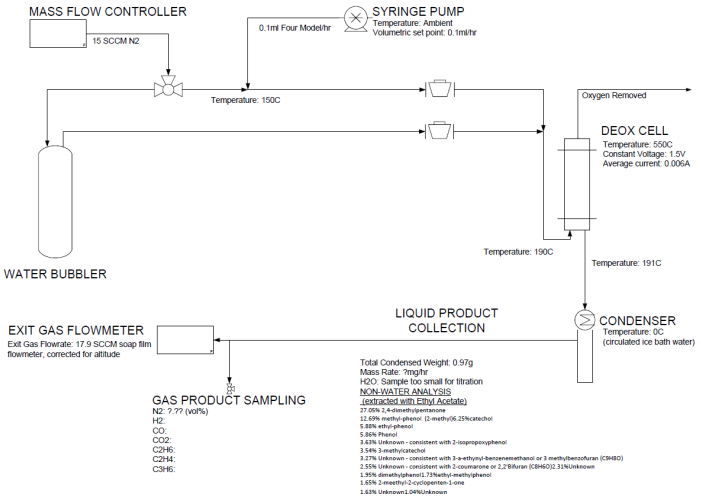

Figure 13. Schematic of 4-model Compound Test

Table 24. Feed and Product Liquid Analysis

	4 Model Feed Compound			4 Model Feed Compound	
Compound	Compound	% by mass	Compound	Compound	% by mass
Syringol		26.78%	Syringol		26.78%
Acetic Acid		26.58%	Acetic Acid		26.58%
2,4-dimethylpentanone		26.78%	2,4-dimethylpentanone		26.78%
Water	H_2O	19.86%	Water	H_2O	19.86%

No Electrode thermal effect 550°C 4-Model Liquid Product	
Sigma-Aldridch	**% Area**
	63.05%
	10.56%
	6.49%
	2.15%
	1.84%
	1.82%
2-hydroxy-4-methoxy-benzaldehyde?	1.60%
3-methyl or 7-methyl-benzofuran	1.09%
	1.00%

550°C, 1.5V, 5mA, 4-Model Liquid Product		550°C, 1.5V, 5mA, 4-Model Liquid Product	
Sigma-Aldridch	**Area %**	Sigma-Aldridch	**Area %**
	27.05%	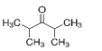	27.05%
	12.69%		12.69%
	6.25%		6.25%
	5.88%		5.88%
	5.86%		5.86%
	3.63%		3.63%
	3.54%		3.54%
	3.27%		3.27%
	2.55%		2.55%
	1.95%		1.95%
	1.73%		1.73%
	1.65%		1.65%

Although syringol was fed to all three tests, it appears in none of the products. Full analysis of these compositions is difficult as the button cell test with such low flow presents difficulty in achieving full mass balance. The gas analysis from these tests are shown in Table 25.

Table 25. Gas Analysis of 4-model Compound Test

No Electrode, 4 model, Product Gas		**1.5V 4 model, Product Gas**	
Compound	**Mass %**	**Compound**	**Mass %**
Hydrogen	1.50%	Hydrogen	2.43%
Methane	2.33%	Methane	2.99%
Carbon Monoxide	16.48%	Carbon Monoxide	15.19%
Carbon Dioxide	6.18%	Carbon Dioxide	23.17%
Ethene	1.54%	Ethene	1.70%
Ethane	6.00%	Ethane	6.43%
Propane	62.70%	Propane	46.77%
Butane	3.27%	Butane	1.31%

STACK IMPROVEMENTS

The focus of the last quarter of 2015 was on improvements of stack test configurations and the overall stack build. These improvements were implemented for the testing reported in this report. In a separate program at Ceramatec funded by NASA, an alternative interconnect material was implemented that provided a better CTE match to the Ceramatec electrolyte. This program requires a robust internal manifolding, and the new interconnect material provided a better seal and overall performance. Figure 14 provides an image of this interconnect. Along with the improved CTE match, this part will also provide a larger active area.

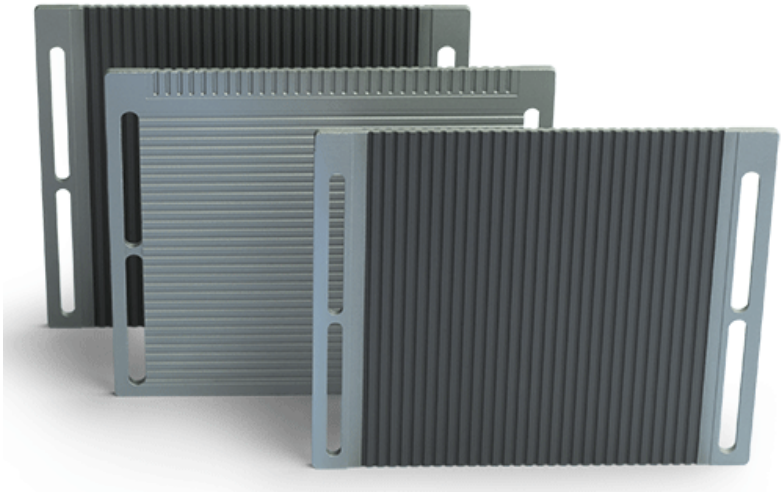

Figure 14. Plansee MK-351 Interconnect Parts (Image provided by Plansee)

A stack using these interconnects (10MK351-550) was built and tested at Ceramatec. This stack was fabricated for the purpose of integrated testing with the fast pyrolysis bio-oil reactor at PNNL. The stack was a 10-cell stack using the new interconnect material with hard glass seals and the copper substituted fuel side electrode. Initial testing at Ceramatec showed good and consistent open circuit voltages, which is a measure of a good seal. Performance was adequate at 550C (the proposed integration test temperature) with an ASR of 28 ohm*cm^2. This electrolysis sweep plot can be seen below in Figure **15**.

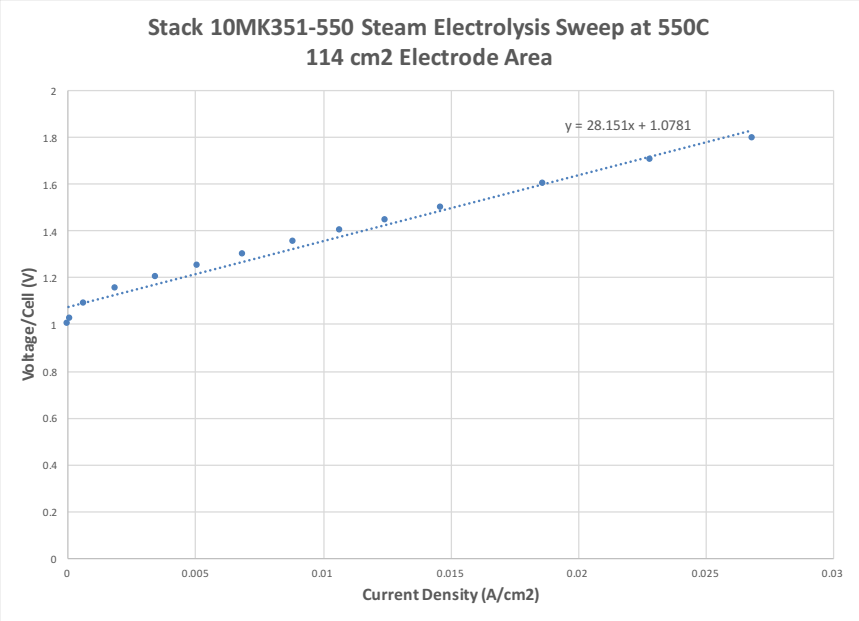

Figure 15. Steam electrolysis sweep of 10MK351-550 at 550C.

Integrated Test

The stack and associated hardware needed to convert the existing stack test stand at PNNL to accommodate the new stack design were shipped to PNNL. An engineer also traveled to PNNL convert the test stand and install the new stack. This entailed removal of some welded components on the old stand and installation of a new base plate. Alteration of the fuel inlet and outlet plumbing was also needed. Figure 16 is a picture of stack 10MK351-550 installed in the test stand at PNNL.

Figure 16. Stack 10MK351-550 installed in test stand at PNNL.

After the fast pyrolysis reactor was modified and approved for safety the stack test stand was connected to it and cold leak checks were performed. Several tests were performed to identify leaks in the stack arrangement and they were fixed to a large extent. The stack was tested 600 °C and at 1.8 V/cell the current was 3.24 A. This performance was in line with that seen in pre-tests. The reactor product slip stream was then added and the hydrogen and water was turned off. The stack began operating on the pyrolysis vapor at 1.8 V/cell and 4.38 A. After about 1 1/2 hours the current increased to 12.7 A. The dry ice trap was found to be clogged. The stack was placed back on steam and the clogged component replaced with a different one that was not likely to clog. Below in Figure 17 and Figure 18 are pictures of the collection in the electrostatic precipitator and the dry ice trap.

Figure 17: Collection of the product post EDOX in the ESP.

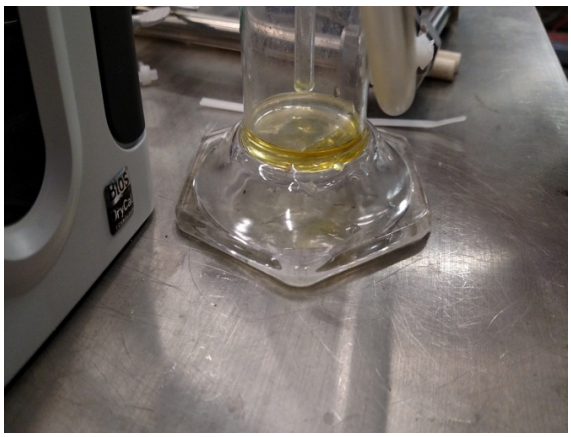

Figure 18: Dry ice trap (thawed) with collected produce post EDOX.

The system was again placed on the fast pyrolysis slip stream and operated to collect more sample at 600 °C, 1.8 V/cell and 12 to 14.6 A. This ran for about an hour and the stack was placed on steam hydrogen/nitrogen and the samples collected. Additional runs of the stack using pyrolysis vapors were successfully made by PNNL personnel at different voltage conditions on subsequent days. The results are summarized in the next section.

Post-test Evaluation

The stack was shipped back to OxEon after the integrated test. Stack faces before and after test are shown in Figure 19. No carbon deposition is seen on the stack faces after exposure to bio-oil vapors at 600 °C.

Visual inspection of cells showed that several had cracks possibly causing leaks during testing. However, only nitrogen was flowed to oxygen evolution side in order to avoid leaks providing oxygen to the bio-oil vapor. Thus, one can assume any change in bio-oil chemistry is either caused by catalytic property of the cathode material in combination with electrochemically produced hydrogen. No obvious sign of carbon deposit was seen on the electrode.

a. Stack prior to integration test b. Stack after integration test

Figure 19. Stack before and after integration test

Advanced Cell Design

While the button cells and stacks showed the feasibility of deoxygenation using the electrolysis process, challenges remain in achieving high current. The cells that were used in this project were developed and optimized for 800 °C operation and integration with the pyrolysis operation require them to be operated at ≤ 600 °C. In order to address the feasibility of improved performance at the lower temperature, a thin electrolyte design was fabricated and tested at different temperatures. The thin electrolyte is supported on the air electrode side.

The performance of the advanced cell design in button cell configuration is compared to the stack that was operated in the integration test in Figure 20. As can be seen, the advanced button cell configuration operated at 600 °C showed an identical performance as the stack at 800 °C. Stacks using the advanced thin electrolyte configuration is expected to have a factor of 10 higher current density (i.e. oxygen removal capability) than the present design. Stack development using the new design is beyond the scope of this project.

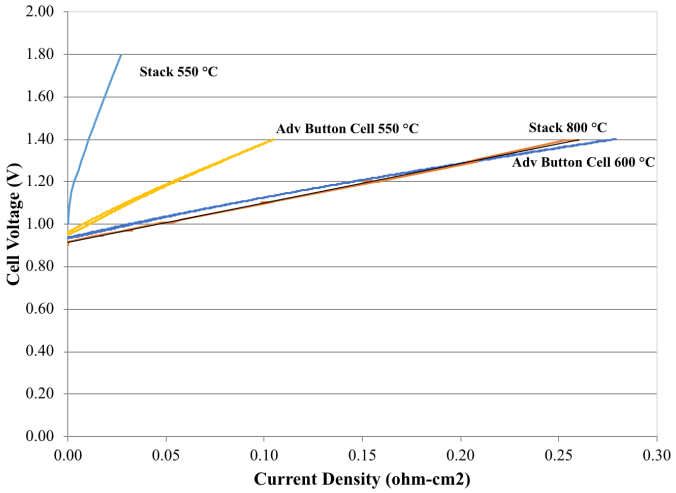

Figure 20. Comparison of present stack performance to advanced button cell configuration

Conclusion – EDOx Cell Testing

A series of tests conducted using model compounds and aqueous fraction of bio-oil demonstrated the potential of the process. Button cells and short stacks of 10-cells were tested with several model compounds and aqueous fraction of bio-oil. Tests using mixtures of model compounds were also performed. All tests showed differing levels of deoxygenation and molecular rearrangement. Depending on the model compounds, 25 to 50% reduction in oxygen content in the product liquid relative to feed was observed Controlling the feed of model compounds was a challenge in these tests. The use of previously developed solid oxide electrolysis cells optimized for 800 °C operation limited the amount of current that could be obtained at a given operating voltage and at the lower temperature of 550 – 600 °C suitable for integration with a pyrolysis unit. An experimental cell design using a thinner electrolyte configuration showed that much higher current, by a factor 10, can be achieved. The new cell design has the capability of significantly higher levels of deoxygenation.

References – EDOx Testing

1. S. Czernik, A.V. Bridgwater, *Energy & Fuels* 18 (2004) 590–598.
2. D. Elliott, Pacific Northwest National Laboratory, personal communication.
3. A. Corma, G. Huber, L. Sauvanaud, P. O'Connor, *J. Catal.* 247 (2007) 307–327.
4. D.C. Elliott, *Energy & Fuels* 21 (2007) 792–1815.
5. Liquid Biofuels, Nexant Inc report, 2006.
6. Adjaye, J.D., Bakhshi, N.N., *Fuel Processing Technology* 45, 1995, 161– 183.
7. Huber et al, I & EC R, 2006, 192
8. E. Tronconi, N. Ferlazzo, P. Forzatti, I. Pasquon, B. Casale, L. Marini, Chem. Eng. Sci. 1992, 47, 2451.
9. Hurff, S.; Klein, M. *Ind. Eng. Fundam*. **1983**, *22*, 426.
10. Laurent, E.; Delmon, B. *Appl. Catal*. **1994**, *109*, 77.
11. Telephonic conversation with a major petroleum refiner, 2013
12. W. Dönitz, E. Erdle and R. Streicher, in *Electrochemical Hydrogen Technologies*, p. 213, Elsevier (1990)
13. M. S. Sohal, J. E. O'Brien C. M. Stoots, J. S. Herring, J. J. Hartvigsen D. Larsen, S. Elangovan, J. D. Carter, V. I. Sharma, B. Yildiz, Critical Causes of Degradation in Integrated Laboratory Scale Cells During High-Temperature Electrolysis, Prepared for the U.S. Department of Energy Office of Nuclear Energy Under DOE Idaho Operations Office Contract DE-AC07-05ID14517 , INL/EXT-09-16004, May 2009.
14. K. W. Ragland and D. J. Aerts, Properties of wood for com- bustion analysis, Bioresour. Technol., 1991, 37, 161–168.
15. A. V. Bridgwater, Review of fast pyrolysis of biomass and product upgrading, Biomass Bioenergy, 2012, 38, 68–94.
16. Tushar Vispute, Pyrolysis Oils: Characterization, Stability Analysis, and Catalytic Upgrading to Fuels and Chemicals, Ph.D. Dissertaion, University of Massachusetts-Amherst, 2011.

Chapter 2. Testing of Electro-Deoxygenation Reactor with a Bench-scale Fast Pyrolysis System

Pyrolysis oil Deoxygenation Technology Background

The state of the art technology for upgrading pyrolysis oil to hydrocarbon fuel is via a two-step hydrodeoxygenation (HDO) process, which can stabilize pyrolysis oil at lower temperature and convert it into hydrocarbon fuel at a higher temperature [2, 4, 6, 7]. However, this process requires a large excess of hydrogen at high pressures and at temperatures where the bio-oil oxygenated compounds are unstable. The catalyst life is also shortened during the process due to sulfur poisoning and coking. This necessitates the use of a multi-stage upgrading process where each step is operated at an increased processing severity and increase challenges for distributed scale-deployment due to high capital and operational cost.

Electrochemical upgrading

This new study then proposes to improve upon the current state-of the art upgrading process that is amenable to distributed scale deployment by minimizing the system foot-print and reduce hydrogen consumption and improve conversion towards high-value chemicals and fuels. This is done by employing solid oxide membrane technology developed by Ceramatec/OxEon discussed earlier. After development of a prototype stack-cell, the unit was then integrated with the PNNL fast pyrolysis system for successful demonstration of the deoxygenation chemistry.

Single stage hydroprocessing thus produces a tar-like product. The catalyst life is also shortened during the process. This necessitates the use of a multi-stage upgrading process where each step is operated at an increased processing severity. Earlier works has been focused on the removal of minerals and contaminants to the catalyst via physical upgrading efforts, such as biomass dusting, fines removal through filtration (both cold and hot methods), ionic exchanges [1] and shows great potential in improving the catalyst lifetime by eliminating minerals deposition into the catalyst. However, biomass also contains sulfur, which is a known poison for many metal-based catalyst. More recent work in the area of chemical stabilization process, was discussed earlier by Wang et al [8] which employed noble metal as a catalyst (Ruthenium), has been focused on hydrogenation of some functional groups that are known to be unstable at high temperatures. The study then proposed engineering approaches surrounding the problem of catalyst deactivation by sulfur poisoning by employing improved guard beds, bed grading and regeneration methods that can extend the lifetime of the catalyst. Properly stabilized, bio-oil can then be processed at high temperatures (400ºC) without problem to undergo deep hydrotreating and hydrocracking to yield upgrading hydrocarbon blend stock. (Figure 21). However, catalyst lifetime on the first stage is yet to be optimized and there are yet more challenges to make it relevant, such as requirement of significant quantities of hydrogen to remove oxygen; economic availability of hydrogen at distributed smaller scale suitable for biomass conversion; and significant process exotherm due to high oxygen removal requirement (25% by mass) requiring high recycle rates are impediments to commercialization of the technology.

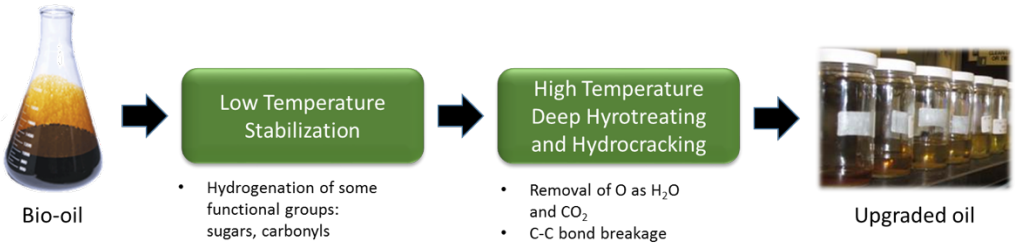

Figure 21. Two-step hydrotreating of bio-oil at PNNL

Methods and Materials

EDOx small-scale reactor development.

EDOx-stack cell testing

In the integrated test conducted at the Pacific Northwest National Laboratory, a slip steam of pyrolysis vapor was fed to the cathode of a 10-cell stack through heated transfer tube. The stack was located in a furnace adjacent to the pyrolysis unit. Deoxygenation tests were conducted at stack operating temperatures of both 550 and 600 °C. The integrated test system is shown in Figure 22.

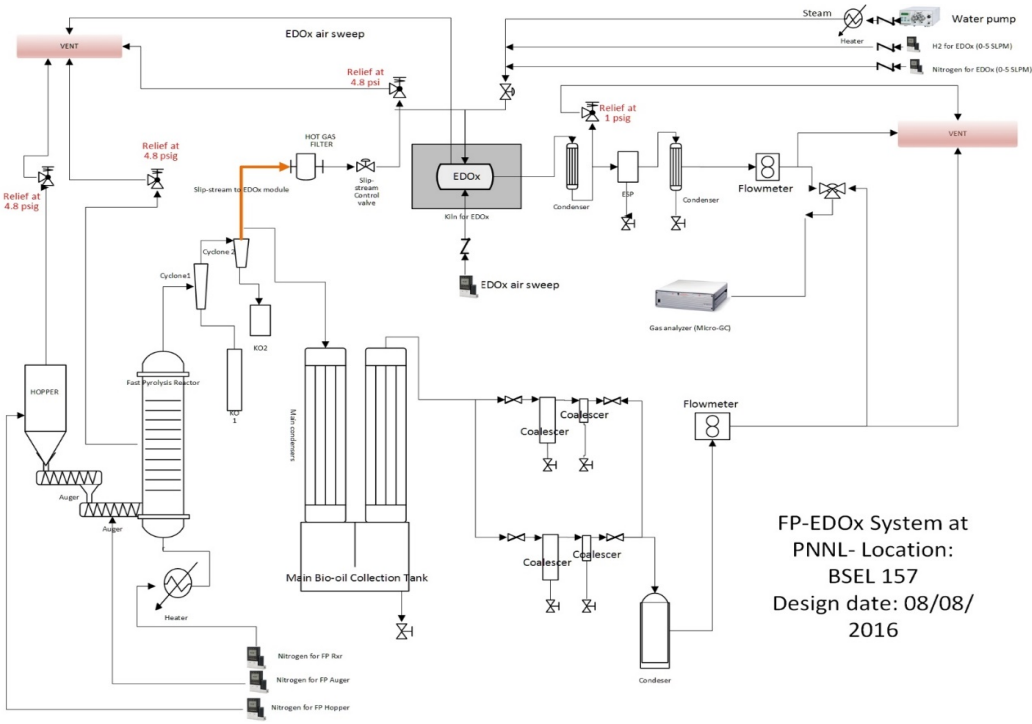

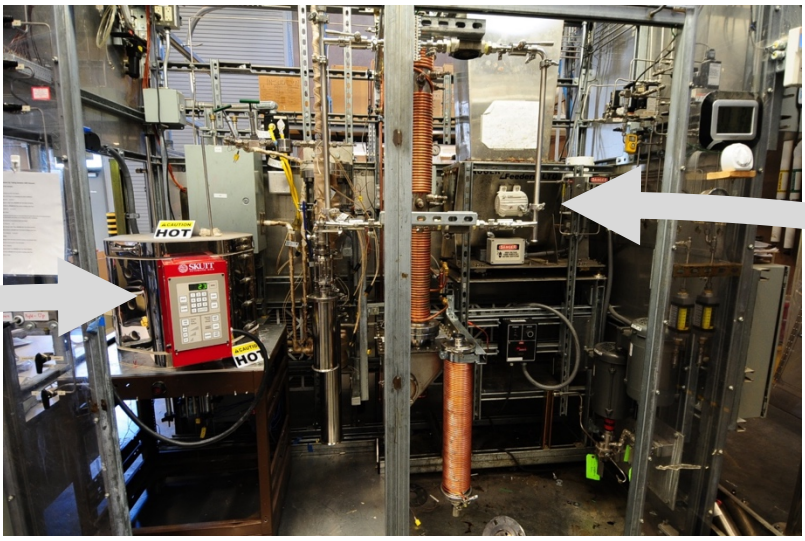

EDOx Stack in Furnace 10-cells Total area ~500 cm^2

Fast Pyrolysis Unit

Figure 22. Integrated Pyrolysis-EDOx Test schematic (above) and set up (below)

Integrated Test of EDOx with fast pyrolysis system.

The fast pyrolysis consists of a feeding system, using two screws: First, the integrated feed screw on a stirred hopper system (Schenk Accurate) meters feed to a second, high speed screw which quickly feeds to the bottom of the fluidized bed on a side port. The stirred hopper has been sealed to operate at 35kPa with minor leakage that is mitigated by metering nitrogen to the hopper. Externally heated nitrogen from a custom non-contact heater is used to fluidize the sand in the pyrolysis reactor, which has operated up to 550°C. The char is separated via heated cyclones operating between 400°C and 500°C. The oil collection system consists of two spray towers followed by multiple traps. First, the gas is quenched to room temperature in a co-current, downflow packed tower. The vapor is further captured in a tertiary collection tower. The remaining balance of light oil, water, are captured in two coalescing filters, the second of which is chilled with dry ice. The off-gas is measured in a wet test meter prior to exhaust. The system has been demonstrated for pine sawdust, and other mixed woody feedstock.

The laboratory scale fast pyrolysis reactor at PNNL was fed Ponderosa pine from American Wood Fiber (AWF) at a rate of 0.9 kg/hr. The feed had been sieved for removal of fine fraction (>100 mesh. Modifications on the system are as follow: 1) Improved fast pyrolysis reactor (FP) design with newly reduced internal volume and gas residence time of below two seconds at full operating temperature (480-500ºC). 2)Newly designed cyclones, with reduced internal frictions in the inlet, and two-stage cyclones, with cyclone 1 with a larger volume, and cyclone 2 with smaller volume, designed to collect smaller sized particles. 3)Hot gas filtration (25-micron sintered metal filter) to ensure capture of fine particles prior to entering the slip-stream to the EDOx. 4)Slip-stream metering valve to ensure proper control of flowrate of slip-stream and to make manual adjustments during the run for constant flowrate with potential changes to back-pressure in the system. 5) Electrostatic Precipitator (ESP) operated up to 15 kV at 0.05 mA to ensure coalescing of the vapors without the added back-pressure typically encountered when using a filter unit.

The fast pyrolysis unit achieved isothermal operating temperature conditions throughout the bed (480 ºC). The gas flow rate was consistent with approximately 70 SLPM, ensuring low gas residence time (<2s). Cyclone 1 and Cyclone 2 was able to collect char, Hot gas filtration functioned as expected and the ESP unit was operated during the test and was found to effectively work about 50% of the maximum output of 30 kV, that is approximately 15 kV. During the operations with the ESP, most of the vapor flow was measured at about 2 SLPM (~3 wt.% of the overall pyrolysis vapor) condensed.

The FP unit was operated at 480 °C and the EDOx stack was operated at 550 and 600 °C. At the higher temperature, initially the stack had an effective total current of ~ 2A, however with subsequent runs, amperage was effectively increased up to 25 A.

Product Characterization Methods

Ultimate analysis & Carboxylic Acid Number (CAN)/Total Acid Number (TAN) & Carbonyl content, and moisture content.

Elemental analysis was done by Ceramatec Inc, Salt Lake City, UT. Carbon, hydrogen and nitrogen were analyzed using ASTM D5373-14, whereas oxygen analysis was done by difference, sulfur analysis was done by ASTM D4239. Moisture analysis was done by Karl Fisher titration method at PNNL. Carbonyl analysis were done at PNNL by the FAIX method (NREL/TP-5100-65888) and CAN/TAN were done at PNNL by Potentiometric titration according to LAP NREL/TP-5100-65890). Water content was determined by Karl Fisher method (ASTM-4928-12).

HPLC (high performance liquid chromatography)

HPLC (high performance liquid chromatography) is equipped with a Waters 2414 refractive index detector. A Bio-Rad Aminex HPX-87H ion exclusion column (300 mm × 7.8 mm) was used for analytes separation. Sulfuric acid (0.005 M) was used as eluent at a flow rate of 0.55 mL/min.

C-13 NMR analysis

Approximately 200 mg of Bio oil sample was dissolved in 0.6 mL of deuterated Dimethyl Sulfoxide (DMSO-d_6) containing 0.05 M $Cr(acac)_3$. ^{13}C NMR spectra were acquired using a Varian Inova 500MHz spectrometer and the chemical shifts were referenced to the residual solvent peak at 39.52 ppm. The ^{13}C NMR spectra indicate an entire carbon content within the bio-oil and the chemical shift range provides the information of functional groups on the structure [14]. Additional to Mullen's characterization of fast-pyrolysis bio-oils by NMR spectroscopy, we also reported carbon assignment of anomeric carbon in sugar at chemical shift between 84-103ppm [15]. Chemical shift / Assignments are listed in Table 26.

Table 26. C13-NMR chemical shift and assignments

C^{13}-NMR Chemical shift	Functional group
180-215ppm	Carbonyl (aldehyde ketone)
163-180ppm	Carboxyl (ester acid)
103-163ppm	Aromatics olefins
84-103ppm	Carbohydrate sugars
54-84ppm	Methoxy/hydroxy
1-54ppm	Alkyl carbons

Computational Methods

Density functional theory calculations.

Periodic density functional theory (DFT) calculations were performed within the generalized gradient approximation with the exchange correlation functional of Perdew, Burke and Ernzerhoff [50] as implemented in the CP2K package[51-52]. Grimme's second-generation corrections were used to take into account dispersion forces or van der Waals interactions to describe energies more precisely.[53] For the core electrons norm-conserving pseudopotentials[54] were used, while the valence wave functions were expanded in terms of double-zeta quality basis sets[55] optimized for condensed systems to minimize linear dependencies and superposition errors. Electrostatic terms were calculated using additional auxiliary plane-wave basis set with a 400-Ry cutoff. The Γ-point approximation was employed for the Brillouin zone integration. For cluster calculations, a dielectric continuum function ($\varepsilon_0 = 72$) was used to represent water solvation[56-57].

Reaction energetics were evaluated using 1 nm (corresponding to 50 atom clusters) metal nanoparticles of Ni as well as a graphene sheet to represent carbon support, C. Similar to our previous work[58-61], all 50-atom electrocatalyst clusters were prepared with an *ab initio* molecular dynamics protocol that involved heating the cluster to 2000 K, propagating the system for ~3 ps, and annealing for ~10 ps until the temperature is below 1 K. A final geometry optimization was used to remove residual forces. Although the protocol does not guarantee a global energy minimum cluster conformation, it does result in a stable low energy cluster. Parameters of the model is listed in **Error! Reference source not found.**.

Table 27. System Parameters for EDOx model development using DFT (Density Functional Theory)

H2O water concentration	**3**	**wt%**
N2 carrier flow rate	1	SLPM
Temperature	550	deg C
metal	Nickel	
structure	<111>	
Thickness	1-10 micron	
Organic substrate	Guaiacol	
Electrode surface area	45	Cm^2
Guaiacol mass fraction in Nitrogen	0.29	
Top 5 products	cathecol, salicyldehyde, Phenol, o-cresol, 2-ethyl-phenol.	

Experimental Results

Four different test conditions were completed to test the integration of fast pyrolysis and the EDOx module. Different conditions, OCV (Open Circuit Voltage), low Amp, mid amp, and high amp) were completed with the following parameters (Table 28). Higher performance (amperage) was seen at at 600 °C.

Table 28. Summary of stack-cell and fast pyrolysis integration test conditions.

LRB#	***Run#***	***Average Current (Amp)***	***Voltage***	***EDOx TOS(h)***	***FP TOS(h)***	***FP gas flow rate (with slip stream) SLPM***	***Slip stream flow rate (SLPM)***
62238-45	*EDOx-low current*	5.2	18	1.95	3.83	60.71	2.008
62238-49	*EDOx-mid current*	6.4	13	2.93	4.92	65.39	2.067
62238-53	*EDOx - high current*	20	15	1.83	3	65.3	1.926
62238-53B	*EDOx-OCV*	0	0	1.38	2.58	65.2	2.448

Resulting process has a mass recovery of 80-90%. Majority of the unrecovered product is water due to absence of efficient water collection system (i.e Drie-rite column or impingers) which can cause system back-pressure and cause leak across the EDOx stack. In these tests, there was negligible leak in the EDOx stack.

Table 29. Yield of EDOx process

	Organic yield (w/w)	***Aqueous yield (w/w)***	***Gas Yield (w/w)***	***Char yield (w/w)***
EDOx-20 amps	0.22	0.17	0.61	N/A
Fast pyrolysis	**0.65**	N/A	**0.11**	**0.24**

In comparison to fast pyrolysis oil quality, when the pyrolysis vapor was subjected to the stack cell at OCV (Open circuit voltage) condition, there is already a 37% deoxygenation of the liquid product relative to feed, which one can expect to be a catalytic process due to the presence of nickel metal on the cathode surface. However, with the added electrical energy input, liquid product showed decreased oxygen content, oxygen removal rate is seen below to be an additional 5% higher than the baseline (OCV). It is apparent that applying electric charge resulted in further product deoxygenation. Furthermore, by applying electric charge on the surface, the product H/C decrease, indicating increased aromaticity of the product.

Table 30. Elemental analysis of liquid product of EDOx process at baseline condition.

Elemental balace (dry basis)	Whole Bio-oil composition	EDOx-OCV Organic Product	Change%	EDOx-15VDC Organic Product	Change%
Carbon	52.8%	67.3%	28%	69.4%	31%
Hydrogen	6.3%	6.5%	3%	6.5%	3%
Oxygen	40.7%	25.6%	-37%	23.6%	-42%

Further summary of the product quality also demonstrates a transformation of the final product oil, especially when observed current is high, resulting not only in decreased oxygen content, but also decreased moisture content and increase of Phenolic acid number, and generally increase in overall total acid number. The increased aromaticity of the product coincides with the increase of the phenolic acid number, further supports the possibility that electrically charged cathode increased in its catalytic functions.

Figure 23is the correlation of level of deoxygenation of the final organic fraction with the observed current across stack cell in Amperes. Moisture content was also plotted to show decreasing trend of as the oxygen content decreases.

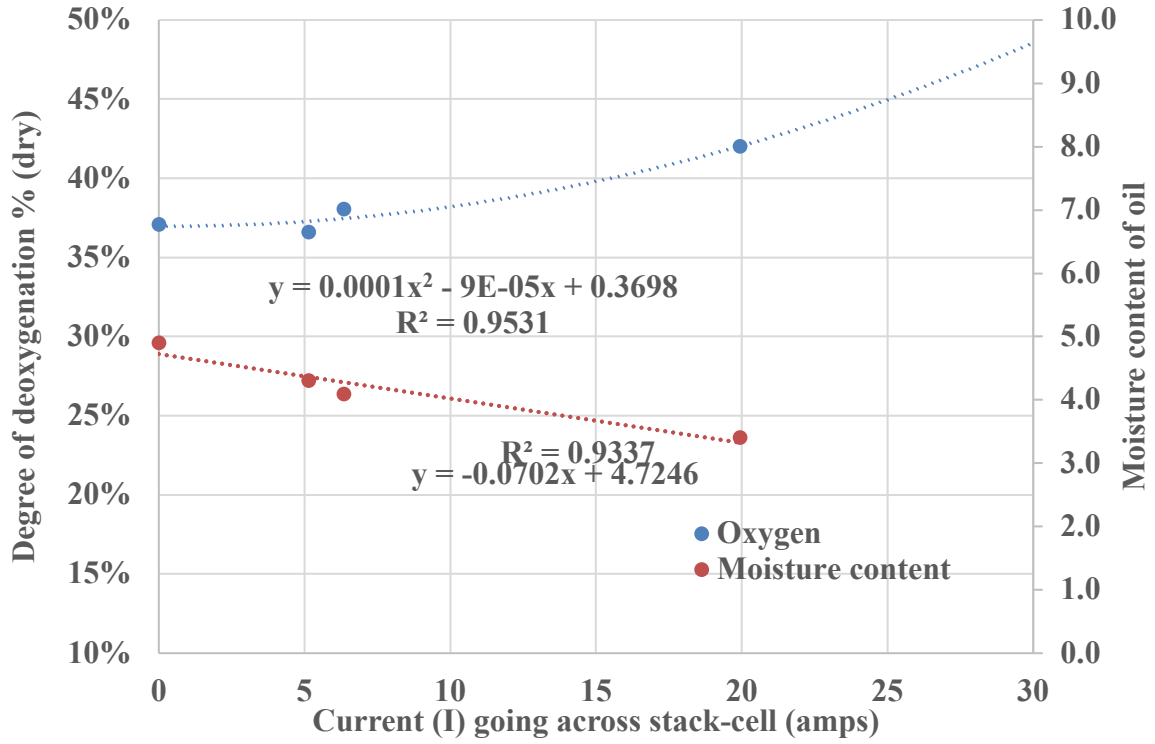

Figure 23. Correlation of Stack Current to Extent Deoxygenation

Increased deoxygenation chemistry on the surface may been resulted by increased aromaticity of the final product and shifted the product distribution, including the acids into more phenolic/aromatic regime, yet still retaining the typical carboxylic acid acids, typically consisting of acetic, formic and propionic acids as seen in relatively stable amount of CAN (Table 31). Carbonyl content of the product didn't display significant change with the current change, indicating that carbonyl-containing species were not much affected by the EDOx process.

Table 31. Product oil quality

Shows differences in elemental analysis (C,H,N,O,S, Moisture), as well as PhAN (Phenolic Acid Number), CAN (Carboxylic Acid Number), and TAN (Total Acid Number) and lastly Carbonyl titration (Faix) was also done to compare quality of final product.

	wt% (dry-basis)					*KF*	*mg KOH/g*		*mmol CO/g*
Current (Amps)	C	H	N	O (by diff)	S	Moisture%	PhAN	CAN	TAN	CO
Raw pyrolysis oil	52.78	6.28	0.09	40.69	0.04	20.6	217.5	60.0	277.5	7.77
0 (OCV)	67.35	6.46	0.57	25.60	0.02	4.9	2003.8	466.5	250.3	2.90
5	67.14	6.36	0.68	25.80	0.02	4.3	2188.4	430.0	261.4	3.17
6	67.98	6.43	0.37	25.20	0.02	4.1	2143.3	396.3	253.5	3.04
20	69.41	6.47	0.50	23.59	0.02	3.4	2233.2	422.9	266.1	2.95

Furthermore, with HPLC of the aqueous product, collected downstream of the ESP, at the condensers, it can also be seen in Figure **24** that concentration of acetic acid increased with higher amperage in contrast with decreasing acetaldehyde, indicating the possibility of enhanced deoxygenation of larger oxygenates components and resulting in increased availability of oxygen radicals that resulted in oxidation of acetaldehyde to form acetic acid.

Table 32. Light components detected by HPLC in the aqueous stream. Main products are acetaldehyde, methanol, and acetic acid. Amount is in wt%, balance is water

Peak Name	*OCV*	*Low Amp*	*High Amp*
Acetalydehyde	6.737	5.629	3.607
Methanol	5.86	7.494	5.319
Acetic acid	5.575	6.77	6.615
Propionaldehyde	1.503	1.088	1.874

acetone	1.128	0.759	0.789
Propanoic Acid	0.906	1.232	1.062
methyl acetate	0.66	0.602	0.663
Glycolaldehyde	0.508	0.507	0.327
MEK (2-butanone)	0.401	0.368	0.31
Ethanol	0.271	0.36	0.154
1,2-butandiol	0.207	BD	0.157
2-cyclopenten-1-one	0.181	0.167	0.142
Crotonaldehyde	0.158	0.062	0.146
Propylene Glycol	0.105	BD	0.243
tert-Butanol	0.096	0.084	BD
1-butanol	0.086	0.059	0.196
Valeraldehyde	0.08	0.074	0.051
1-propanol	0.074	0.037	0.17
2-methylcyclopentanone	0.07	0.074	0.05
Phenol	0.05	0.035	0.079
3-methyl-2-cyclopentene-1-one	0.045	0.045	0.039
3-hexanone	0.012	BD	BD

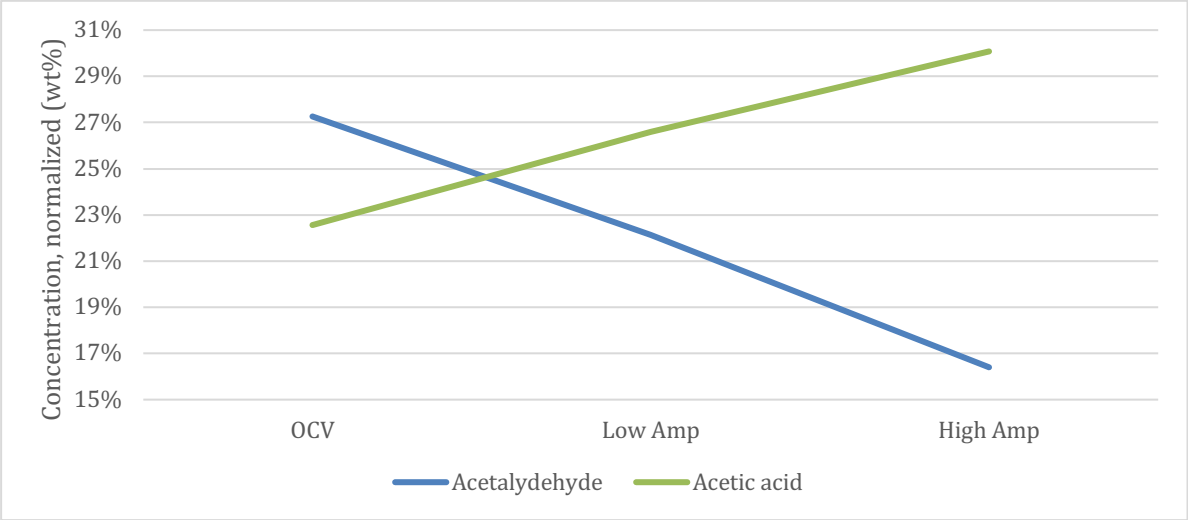

Figure 24. Opposite trend of main species of oxygenates within the aqueous product of EDOx process

Gas analysis

From the fast pyrolysis process, seen in Table 33 , evidently some methane, CO2 and CO were formed, mainly from cracking, decarbonylation and decarboxylation that took place within pyrolysis process, typically catalyzed by the presence of alkali and alkali-earth metals present in the biomass.

Table 33. Gas analysis of EDOx process of non-N_2 gases

NON-N2 GASES	H2	CH4	CO2	CO	C2+	C3+	C4+	C5+
FP ONLY	0.00	16.21	39.08	44.71	ND	ND	ND	ND

EDOX-OCV*	65.47	2.41	2.90	13.79	0.92	2.33	6.51	5.67
EDOX-15V	24.22	2.73	3.30	14.28	1.17	1.97	3.23	2.30

*Hydrogen gas was added to assist with Ni reduction on the surface.

Furthermore, thermal conversion of bio-oil vapor alongside with the NCG from the fast pyrolysis is seen at EDOx-OCV (Open Circuit Voltage), where no electric charge is applied, but it is seen that further cracking reaction occurs, as the formation of small hydrocarbons such as methane, ethane, ethylene, propane, propylene, isobutene, butane, butenes and pentanes were detected at significantly higher level than that of fast pyrolysis (Table **33**), which can be attributed to the presence of Ni-catalyst on the cathode surface.

However, when electric charge is applied on the cathode surface (EDOx-15V), we observe significant formation of hydrogen from electrolysis of water and increased formation of CO (Carbon monoxide), CO_2 and methane when compared to OCV condition, indicating a significantly higher degree of decarbonylation/decarboxylation (Table 34) from biomass oxygenates, and higher degree of cracking to lighter components.

Table 34. Gas analysis of EDOx, non-N_2 and non H_2 gases

NON-N2 GASES	CH4	CO2	CO	C2+	C3+	C4+	C5+
FP ONLY	16.21	39.08	44.71	ND	ND	ND	ND
EDOX-OCV	6.98	8.39	39.93	2.67	6.75	18.86	16.41
EDOX-15V	9.43	11.39	49.28	4.03	6.78	11.17	7.93

Furthermore, C13-NMR analysis of the functional groups were done on the product processed with the highest EDOx severity to be contrasted with baseline (no voltage). Compared to the controls, EDOx process resulted in higher aromatic content, decrease of carbohydrates and methoxy/hydroxy group, indicating a distribution shift of the product, where some carbons that were more linear, now were converted to more aromatic (Figure **25**). Thus, it is observed there is a clear trend of oxygen in the form of decarbonylation or decarboxylation.

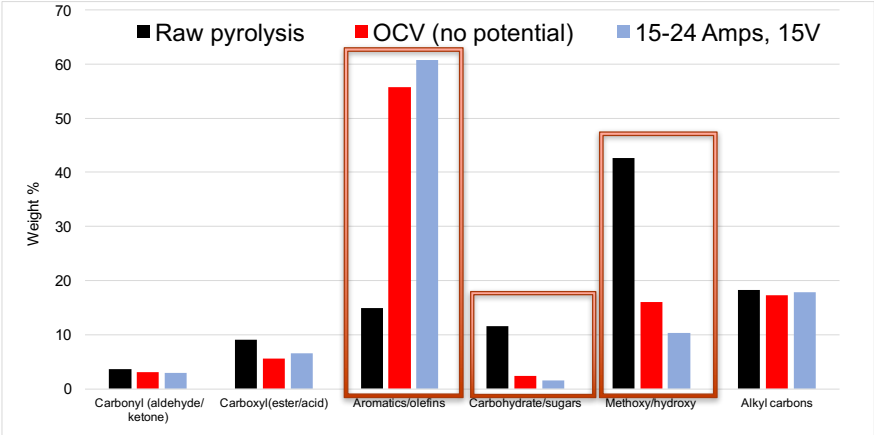

Figure 25. C13-NMR analysis of liquid product from pyrolysis oil, and EDOx process. Red box indicates most significant change in product.

Discussion

As seen in the C-13 NMR and elemental analysis, there was a significant deoxygenation that occurred with the presence of electricity on the surface. However, it is challenging to pin-point which deoxygenation mechanism occurred at the surface without discussing possible mechanisms on a fundamental level. In order to elucidate the mechanism of deoxygenation, it is postulated that firstly electro-deoxygenation would have occurred in the Nickel catalyst surface. On that assumption, a first principle surface chemistry

calculation was accomplished by leveraging high performance computing available at PNNL to perform a a DFT modelling (PNNL Institutional Computing) to demonstrate that removal of oxygen group from an oxygenate substrate.

The following hypothesis was tested, where hydrodeoxygenation of pyrolysis oils is representing transformation of phenolic compounds such as guaiacol on a simplified nickel surface, Ni <111>. Secondly, to demonstrate effect of a charged metal surface on the oxygenate, we also assumed that higher hydrogen efficiency is predicted to be most favorable in the vertical orientation, where the oxygen-containing hydroxy, or methoxy group are facing towards the charged surface (Figure **26**).

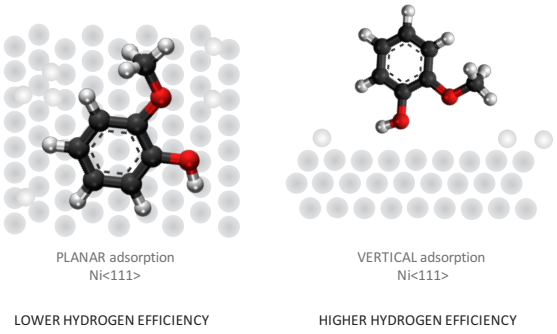

Figure 26. Guaiacol orientation on Nickel catalyst surface

Combining both experimental work with computational work at PNNL and OxEon, we tested and found that the original hypothesis of guaiacol conversion to phenol and to benzene (Guaiacol->Phenol) is possible with the application of charge on the surface. Specifically, with the catalyst surface being applied with charge, guaiacol orientation approaches at an angle (Figure **27** and Figure **28**), resulting in higher contact probability of the hydroxyl group to the surface. And thus, charged surface increase the probability of deoxygenation by lowering the bond dissociation energy (BDE) resulting in dehydroxylation and removal of an oxygen atom, as seen in **Error! Reference source not found.**.

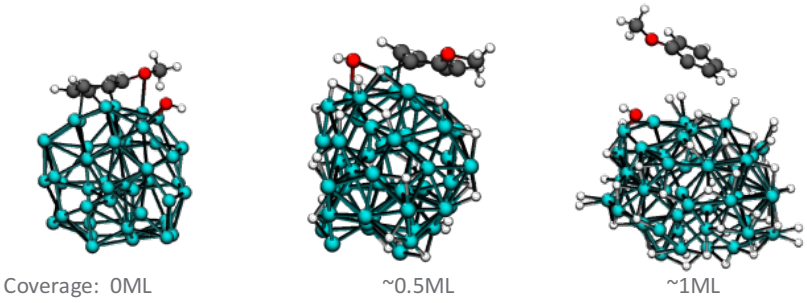

H Coverage	BDE (no charge) (in Kcal/mol)	BDE (charged) (Kcal/mol)
0	-2	0
0.5	24	0
1.0	32	34

Figure 27. Guaiacol orientation towards charged nickel surface is angled.

At OCV, or no voltage, guaiacol orientation is planar towards the catalyst surface (Figure 28). This results in higher probability of hydrogenation of the ring, resulting in ring saturation, and therefore a lower hydrogen efficiency as the final product have lower energy density than aromatic products. (i.e cyclohexane has lower energy density than benzene).

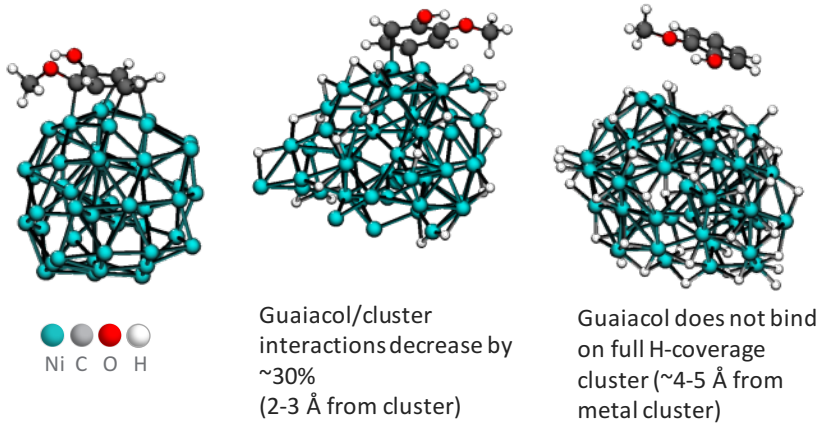

Figure 28. Guaiacol orientation towards nickel surface is planar at OCV (open circuit voltage).

In conclusion, a novel solid state electrochemical device was used to remove oxygen from bio-oil, and bench scale testing demonstrated significant changes caused by EDOx, resulting in higher degree of deoxygenation- validating the proposed the technology. In addition, Initial deoxygenation mechanism is proposed via first principle calculation showing that EDOx derived fuels and chemicals can be produced with high hydrogen efficiency, which has potentially lower environmental footprint compared to HDO process and conventional fuel. Future work will be to evaluate new catalytic materials and process optimization schemes for improvement of the deoxygenation process to produce hydrocarbon fuels and chemicals.

Conclusion – Integrated Stack – Pyrolyzer Testing

Integrated testing of stack-cell EDOx reactor was done successfully with the fast pyrolysis system to test conversion of pyrolysis oil vapor to an upgraded liquid product while displaying significant level of deoxygenation. As a result, correlation of pyrolysis oil deoxygenation with the stack current (Amperes) were proposed. Liquid and gas yields were also estimated, and product analysis was done to provide a clear baseline performance for future development of the EDOx process. In addition to the experimental work and results, computational chemistry work at PNNL also demonstrated the feasibility of deoxygenation exists via dehydroxylation of the oxygenates (Guaiacol → Phenol) present in the pyrolysis vapor by using DFT (Density Functional Theory). This was also confirmed by ^{13}C NMR analysis of the liquid product with the decrease of carbon-hydroxyl (C-OH) group in the product. Future work will be to evaluate new catalytic materials and process optimization schemes for improvement of the deoxygenation process to produce hydrocarbon fuels and chemicals.

References – Integrated Testing

1. Zacher, A.H., et al., A review and perspective of recent bio-oil hydrotreating research. Green Chem., 2014. 16(2): p. 491-515.
2. Elliott, D.C., et al., Catalytic Hydroprocessing of Fast Pyrolysis Bio-oil from Pine Sawdust. Energy & Fuels, 2012. 26(6): p. 3891-3896.
3. Elliott, D.C., et al., Catalytic hydroprocessing of biomass fast pyrolysis bio-oil to produce hydrocarbon products. Environmental Progress & Sustainable Energy, 2009. 28(3): p. 441-449.
4. Elliott, D.C., Historical Develpments in Hydroprocessing Bio-oils. Energy & Fuels, 2007. 21: p. 1792-1815.
5. Jones, S.B., Process Design and Economics for the Conversion of Lignocellulosic Biomass to Hydrocarbon Fuels. 2013, PNNL.
6. Corma, A., et al., Processing biomass-derived oxygenates in the oil refinery: Catalytic cracking (FCC) reaction pathways and role of catalyst. Journal of Catalysis, 2007. 247(2): p. 307-327.
7. Huber, G., I&EC R, 2006: p. 192.

8. Wang, H., et al., Bio-oil Stabilization by Hydrogenation over Reduced Metal Catalysts at Low Temperatures. ACS Sustainable Chemistry & Engineering, 2016. 4(10): p. 5533-5545.
9. J.D. Adjaye, B., N.N., Fuel Processing Technology, 1995. 45: p. 161-183.
10. E. Tronconi, N.F., P. Forzatti, I. Pasquon, B. Casale, L. Marini, Chem.Eng.Sci, 1992. 47: p. 2451.
11. Saidi, M., et al., Upgrading of lignin-derived bio-oils by catalytic hydrodeoxygenation. Energy & Environmental Science, 2014. 7(1): p. 103-129.
12. S. Elangovan, D.L., J. Hartvigsen, J. Mosby, J. Staley, J. Elwell, M. Karanjikar, Electrochemical Upgrading of Bio-Oil. ECS Transactions, 2015. 66(3): p. 1-9.
13. W. Dönitz, E.E., R. Streicher, Electrochemical Hydrogen Technologies. 1990: Elsevier.
14. Fulmer, G.R., et al., NMR Chemical Shifts of Trace Impurities: Common Laboratory Solvents, Organics, and Gases in Deuterated Solvents Relevant to the Organometallic Chemist. Organometallics, 2010. 29(9): p. 2176-2179.
15. Mullen, C.A., G.D. Strahan, and A.A. Boateng, Characterization of Various Fast-Pyrolysis Bio-Oils by NMR Spectroscopy. Energy & Fuels, 2009. 23(5): p. 2707-2718.

Chapter 3. Life Cycle Assessment and Techno-Economic Analysis

PROJECT SUMMARY

Upgraded bio-oil produced from fast pyrolysis of biomass was evaluated using electrochemical deoxygenation (EDOx) at a scale of 300 dry metric tons biomass per day (MTPD) and compared to hydrodeoxygenation (HDO) produced at 2000 MTPD. EDOx uses catalytic electrode membranes on a ceramic, oxygen-permeable support, to generate hydrogen in-situ for deoxygenation at the cathode and oxygen removal at the anode. We analyze the life cycle greenhouse gas (GHG) emissions and scale effects of gas-phase upgrading of pyrolysis oil using partial and full upgrading via EDOx and compare it with the large scale HDO process (2000 MTPD). A techno-economic analysis (TEA) model was constructed using Aspen Plus software and experimental data from collaborators on this project (PNNL and OxEon, formerly Ceramatec) to estimate mass and energy balances for the EDOx process and the minimum fuel selling price (MFSP). We observe that the EDOx configurations have lower life cycle GHG emissions of 5–8.4 g CO_2 eq. and 7.4–11 g CO_2 eq. per MJ of a vehicle operated with diesel and gasoline, respectively compared to HDO (39 gCO_2 eq. per MJ). Furthermore, the EDOx processes offers potentially10 times more small-scale pyrolysis upgrading facilities in the U.S. compared to HDO, suggesting that small-scale on-site EDOx processes can reach more inaccessible forest biomass resources. Results of the TEA modeling suggest a MSP of of $1.89/gal based on Aspen Plus models that incorporated the experimental data developed during the project (a 300 metric ton/day facility with 10% IRR using 2015 dollars were the other major assumptions).

Two manuscripts detailing the LCA and TEA work are under development. The manuscript on LCA (Sorunmu et al., 2018) is under revision and the TEA paper is in preparation (Torelli et al., 2018).

Life Cycle Assessment

The objective of the life cycle assessment (LCA) segment of this CHASE project was to apply LCA to compare partial and full EDOx at small scale (300 MTPD) with HDO at large scale (2000 MTPD). The partial EDOx process integrated EDOx upgrading to 33% oxygen removal, analogous to the HDO first deoxygenation unit, and HDO upgrading to complete oxygen removal using the second deoxygenation unit (hydro-treater configuration) described by Jones et al. (2009) for HDO upgrading. The comparison quantifies the GHG emissions from biomass collection to vehicle operation of the three processes.

Aspen Plus models were simulated to generate mass and energy balances based on experimental data, which were then integrated into a life cycle inventory (LCI) model simulated using SimaPro v.8.3 LCA software. Figure 29 shows the process flow diagrams for the three pyrolysis oil upgrading systems compared.

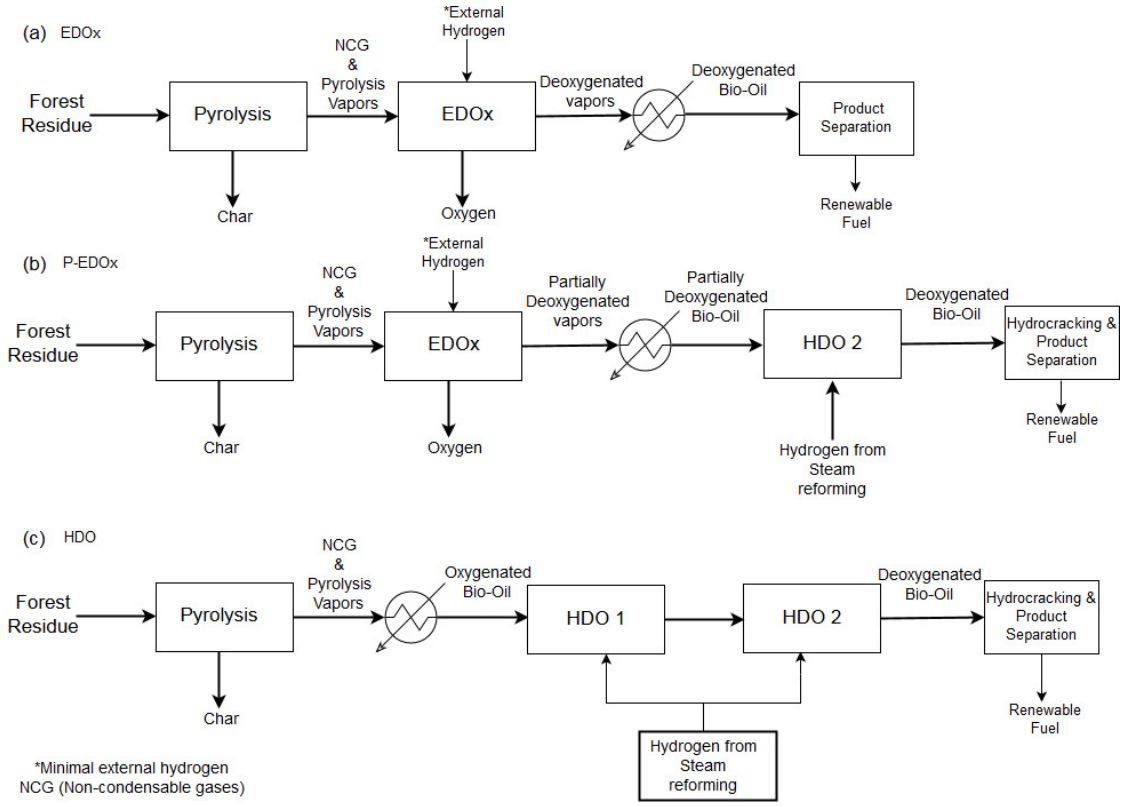

Figure 29. Process flow diagram for: a) electrochemical deoxygenation, b) partial electrochemical deoxygenation, and c) hydrodeoxygenation processes

Life Cycle Assessment Model

The LCA modeling follows the guidelines of the International Organization for Standardization (ISO, 2006). Simapro v.8.3 (Pre, 2014) LCA modeling software is used to develop and link the unit processes for biomass production and transportation, bio-oil production, bio-oil upgrading, product distribution and vehicle operation.

The system boundary (Figure 30) illustrates the processes from the harvest of forest residue to vehicle operation. We use the IPCC 2013 GWP 100a metric to identify the environmental impact of the processes with functional units per MJ of fuel produced and per km of distance driven. This study uses system expansion to handle all co-products. The feedstock is harvested, pre-processed, and transported to a pyrolysis conversion site. There, the biomass undergoes pyrolysis, the vapor of which is available for deoxygenation via EDOx and partial EDOx. In the HDO process, the pyrolysis vapor is condensed before upgrading in two hydrotreaters (Fig. 2). After upgrading and product fractionation, the renewable diesel and gasoline products are distributed and used to operate an automobile with a fuel economy of 10.8 km l^{-1} and 13 km l^{-1} of gasoline and diesel type vehicles respectively. Although the upstream operations in the three processes (EDOx, partial EDOx and HDO) consist of the same operations, they supply feedstock at

two different scales (EDOx and partial EDOx operate at 300 MTPD while HDO operates at 2000MTPD). In the EDOx process, since we assume full deoxygenation by the EDOx unit, after complete deoxygenation, the fuel produced is transported to the refinery for product separation followed by distribution to the market and consumer use in a vehicle. In the partial EDOx process, the delivered feedstock is pyrolyzed and partially deoxygenated to a stable bio-oil via the EDOx process, and then transported to a petroleum refinery for HDO processing in a second hydrotreater to fully deoxygenate the partial EDOx oil. In this case, we assume the EDOx site is in the same location or in very close proximity to the HDO unit at the refinery; hence, transportation distance is negligible. Unlike the EDOx, the partial EDOx requires some external hydrogen for further deoxygenation with a hydrotreater. After HDO deoxygenation, the pyrolysis oil is separated, distributed to the consumer and used for vehicle operations. Electricity needed for the EDOx and HDO unit is assumed to be generated from the average US electricity grid. Although a sensitivity analysis described later, examines the effect of location on the GHG emissions by varying regional electricity grids.

For the HDO process, we used the results of the LCA published by National renewable Energy Laboratory (NREL) detailed in Hsu et al. without any modifications.

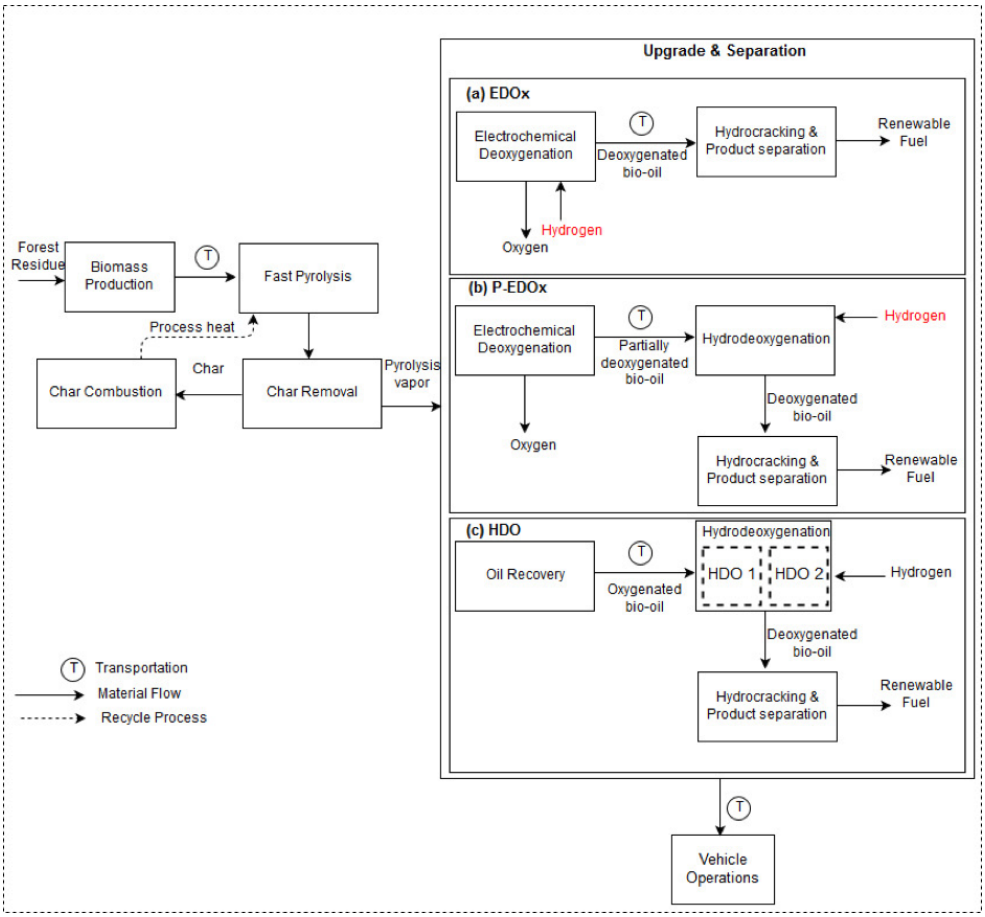

Figure 30. System boundary diagrams for (a) electrochemical deoxygenation, (b) partial electrochemical deoxygenation and (c) hydrodeoxygenation.

In the partial EDOx process, the insertion point (the point where the oil goes to the refinery) is a stable oil produced by the EDOx process that can be easily transported to a refinery for further upgrade/processing. In the full EDOx process, the insertion point is a near finished fuel/blend stock that requires minimal processing in a refinery.

Results and Discussion

Biomass Supply

There is much availability of forest residues across the United States (Figure 31a), where 216 locations can supply feedstock at 300 MTPD for EDOx facilities and 18 locations can supply feedstock at 2000 MTPD for HDO facilities. The map also shows GHG intensity (kg CO_2 eq. per metric ton) of the relevant grid with the darker colors indicating a higher environmental impact. The results show that the North East region that utilizes the Northeast Power Coordinating Council (NPCC) grid has low GHG emissions while fulfilling the biomass supply needed for the siting of an EDOx pyrolysis unit facility but the most feasible location would be in the south, specifically Arkansas and Louisiana due to biomass availability, numerous EDOx locations and close proximity to petroleum refineries. To fulfil the partial-EDOx process mechanism, we used red dots and green lines on the map to represent petroleum refineries and crude oil pipelines, respectively. The presence of a petroleum refinery in close proximity to EDOx sites will enable efficient transport of the bio-oil produced from the EDOx pyrolysis sites to a petroleum refinery for further deoxygenation and separation. If the EDOx process can fully deoxygenate the bio-oil, then the deoxygenated bio-oil will be infrastructure compatible and can be directly added to the crude oil pipeline. The map also shows that when the feedstock transportation radius declines from 80.5 km to 32.2 km (Fig 3b), there will not be any HDO sites to accommodate feedstock supply within this smaller radius but there will still be over 300 EDOx sites (represented in yellow boarders in Figure 31b) to accommodate this smaller supply radius.

(a)

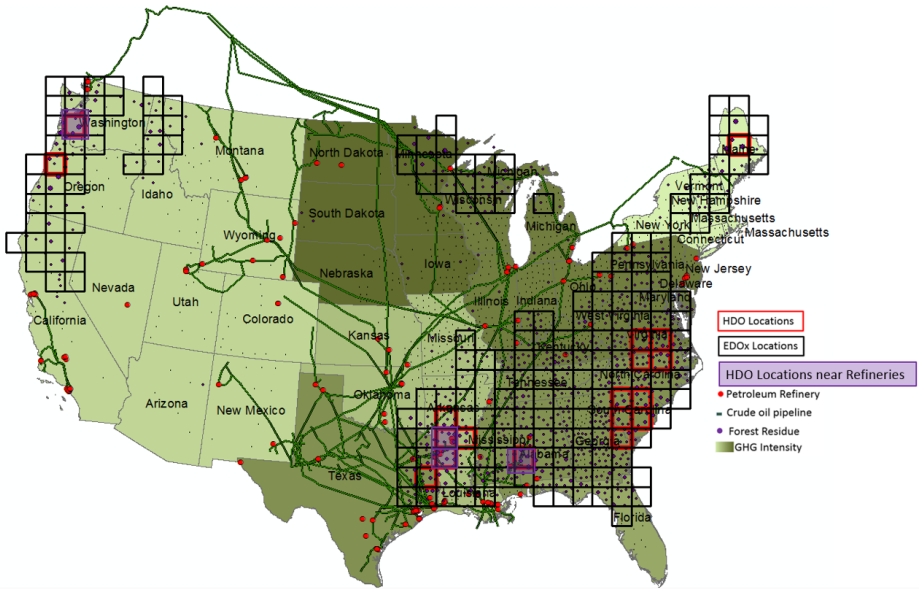

(b)

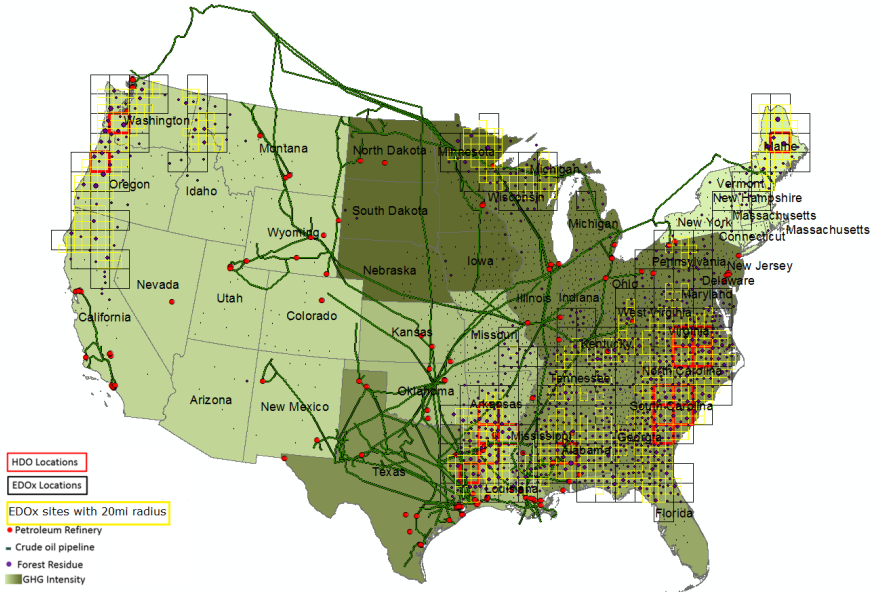

Figure 31 U.S. map showing EDOx and HDO locations and GHG intensity

(a). U.S. map showing EDOx and HDO locations as well as the GHG intensity in CO_2 eq. per metric ton varying by the different electricity grids, forest residue availability in bone dry ton per year (BDTPY), petroleum refineries and pipeline locations. The lighter green indicates a lower GHG intensity and the darker green indicates a higher GHG intensity. The black grid represents the potential EDOx sites while the red grid represents the potential HDO sites. The purple highlights represents HDO locations near refineries **(b)** U.S. map showing the EDOx and HDO sites with the yellow boarders representing a feedstock transportation radius of 32.2km (20 miles).

Greenhouse Gas Emissions

Life Cycle GHG emissions of the three processes

Figures 4a and 4b show that GHG emissions from the EDOx process is lower than the HDO process. In all the results, diesel produced from the EDOx and partial EDOx processes (8.36 g CO_2 eq. and 4.95 g CO_2 eq. per MJ) have lower GHG emissions than gasoline produced from the same processes (10.9 g CO_2 eq. and 7.43 g CO_2 eq.) per MJ of vehicle operation due to the higher fuel efficiency of diesel engines compared to gasoline engines (Hsu, 2012). The partial EDOx upgrading process produces the least amount of GHG emissions due to a lower demand of external hydrogen and electricity than the HDO process and EDOx respectively. Vehicle operation contributes the largest emissions in the partial EDOx process; however, those emissions are biogenic and offset by CO_2 uptake during biomass growth (Han et al. 2011). Oxygen is co-produced in the full EDOx and partial EDOx processes and credited, assuming it displaces oxygen produced via cryogenic processing. The GHG emissions in the pyrolysis and upgrading process are highest for the EDOx system mainly due to the electricity and additional hydrogen required for deoxygenation owing to the limited amount of water in the bio-oil for hydrogen production (shown in SI Table S.4). Although GHG emissions for the full EDOx process are high, the credit from co-produced oxygen is considerable towards reducing net GHG emissions. Overall, the net GHG emissions for the partial and full EDOx processes are lower than the net GHG emissions from the HDO process. When considering the sensitivity of the feedstock collection radius, with lower and upper bounds set to 32.2 km and 950km (the maximum refinery distance), GHG emissions from the full EDOx and partial EDOx processes remain lower than those of HDO process (Figure 32a).

In comparison to conventional fuels on a per MJ basis, GHG emissions for the pyrolysis fuels produced through the partial EDOx and full EDOx processes are 88% to 95% lower than conventional gasoline and diesel GHG emissions (91 g CO_2-eq. and 94 g CO_2-eq. per MJ) based on GREET data (Wang, 2015). This reduction exceeds the Renewable Fuel Standard (RFS-2) requirements which states that the life cycle GHG emission reduction threshold for any advanced biofuel is 50% (U.S. DOE, 2006). While all pyrolysis and upgrading processes would meet the RFS2, the EDOx and partial EDOx upgrading processes are 68-72% and 78-84% lower than HDO upgrading.

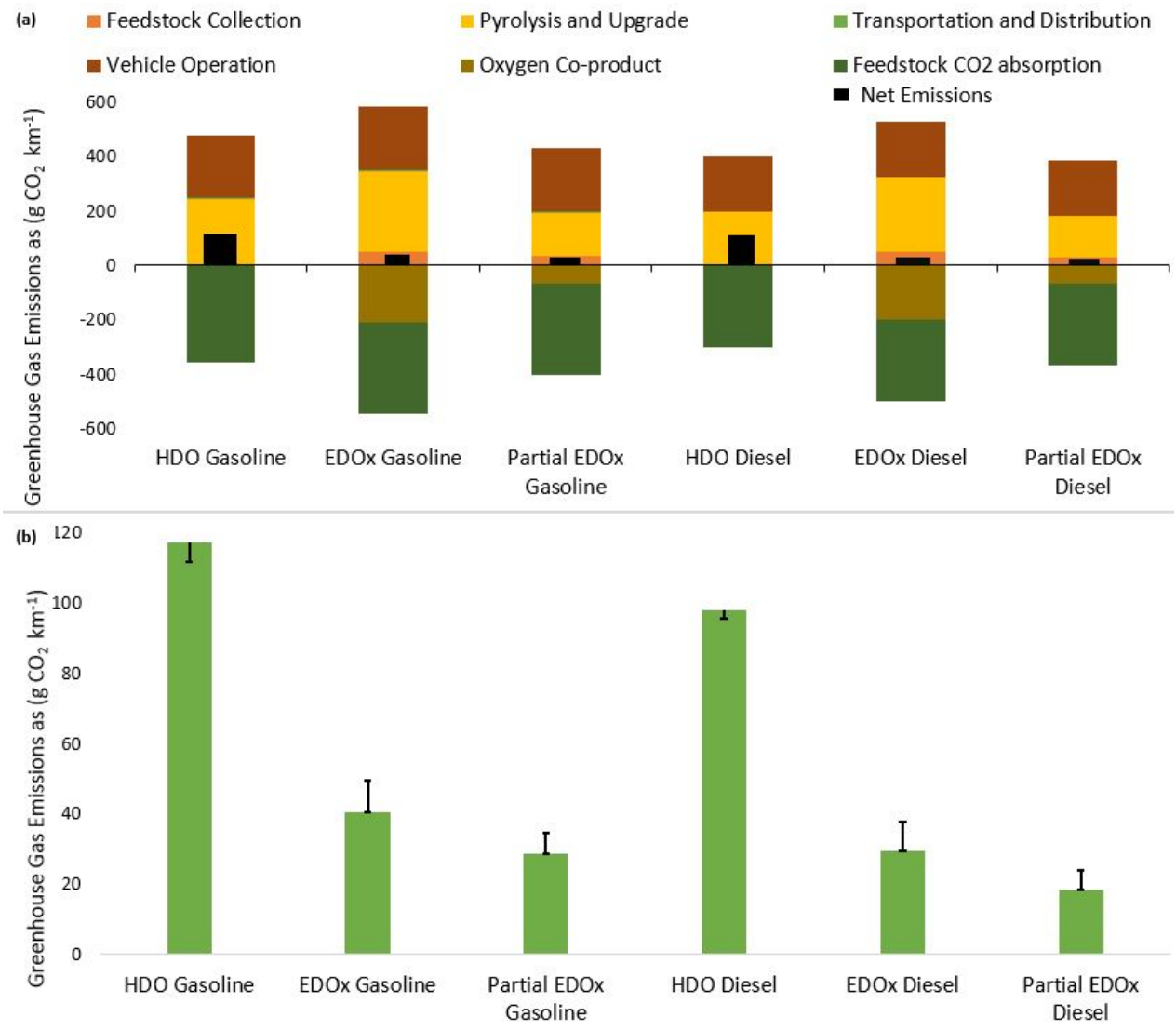

Figure 32. (**a)** GHG emissions for a U.S passenger car operated over a distance of 1km using pyrolysis fuel from different processes. (**b)** Net GHG emissions for a U.S passenger car operated over a distance of 1km using upgraded pyrolysis fuels from different processes.

This figure estimates the GHG emissions for the whole process from feedstock collection to transportation and distribution including oxygen as a co-product. Error bars show lower and upper bounds. The EDOx lower bound represents the GHG reduction limit for a smaller feedstock supply radius of 32.2 km from 80.5 while the upper bound represents the maximum refinery distance from the upgrade units. The HDO lower bound represent the GHG emissions from the use of biomass-derived electricity as feedstock while the baseline represents GHG emissions from grid electricity.

Techno-Economic Analysis (TEA)

Experimental research undertaken in August and September of 2017, in which experimental data from PNNL's stack tests were parameterized into an Aspen Plus model from which capital and operating costs

were estimated for the EDOx upgrading of pyrolysis bio-oil treated at PNNL. The pyrolysis facility operates at a scale of 300 dry metric tons per day/MTPD.

Model of Full EDOx in Aspen PLUS

Traditional hydrotreating contains hydrotreater reactors (HDOs) operating at high temperature and pressure; oxygen molecules where double bonds are removed via H_2 consumption (upgrading). Here, the full EDOx process model in Aspen Plus contains an EDOx reactor, which contains cell-stacks with a permeable O_2 membrane catalyst and consumes electricity to facilitate oxygen removal, that replaces the traditional HDO upgrading. Supplemental external hydrogen is needed in the EDOx reactor to completely deoxygenate the compounds in the reactor. In-situ hydrogen generation is received in the EDOx reactor from the photoelectrochemical (PEC) reactor. The in-situ hydrogen generation is dependent on the initial water fraction in the bio-oil feed from upstream fast pyrolysis (FP) drying process. The entire EDOx process also contains three separators, one heater, and a water splitting PEC reactor. All separators were assumed to have 100% separation of binary components (i.e. water from oil or O_2 from H_2).

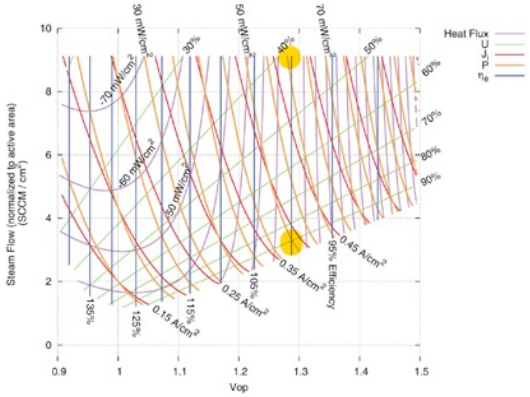

Figure 33. SOEC performance map. Taken from Milobar et al. (2015).

Mass and energy balances were used to size all six process units. Holding time and orientation of separators were used as inputs to complete the sizing procedure. The PEC reactor was sized accordingly via the Type 1 reactor, continuous baggie system configuration, found in James et. al. (2009). The EDOx reactor was sized with respect to the SOEC performance map by Milobar et. al. (2015), shown here as **Error! Reference source not found.**, where a maximum inlet flow rate of 10 SCCM/cm^2. The 10 SCCM/cm^2 is normalized to the active area of 225 cm^2 per cell thus the actually steam flow rate through the system is 2250 SCCM. Milobar et. al. describes the SOEC system as 4 stacks of solid oxide cells, each with 225 cm^2. Variables, *U* (steam utilization), *Ji* (current density), *P* (power density) and *ηe* (stack efficiency) are shown in **Error! Reference source not found.**. The following steps were executed to size the EDOx reactor in the full EDOx process scenario bio-oil deoxygenation as a preliminary approach. Selected desired stack efficiency (η = 100%). Appendix A details the steps taken to size the EDOx reactor and estimate its capital costs.

Capital Cost

Capital cost was executed through the Scale-Up Equipment Cost in Equation 1 found in Jones et. al. (2009). Where n is the scaling factor which ranges between 0.6-0.7. All capital cost for common equipment uses 0.6. Only the EDOx reactor a scaling factor of 0.7. The installation cost factor used was 1.4 to account for

an additional 40% of the capital cost to be the cost of installation for all equipment. The separators (3) scale-up use the design factor found in Jones et. al. (2009), process heater from Dutta et. al. (2015), PEC reactor information and details from James et. al., and EDOx sizing and metrics from Milobar et al. (2015). Note that the capital cost for the EDOx reactor uses Equation 1 and not its required insulation and heat exchanger. The estimated cost for the insulation and heat exchanger is 80% of the uninstalled cost of the EDOx reactor. Then, both EDOx reactor along with the insulation and heat exchanger were multiplied by the 1.4 installation factor to yield the capital cost for the EDOx Reactor System.

$$Scale\text{-}Up\ Equipment\ Cost = Base\ Equipment\ Cost \left(\frac{Scale\text{-}Up\ Capacity}{Base\ Capacity} \right)^{n}$$

Equation 1

All USD amounts were converted from base year dollars to 2011$ and 2015$ to be able to compare across sources with similar pyrolysis processes in comparable dollar amounts. An example of a table using Equation 1 and converting to different USD dollars is found in Figure 3. The conversion is used from the Inflation Calculator, which uses raw data from the Bureau of Labor Statistics' Consumer Price Index (CPI).

The total capital cost of all equipment is calculated by Equation 2 found below. Here, BMC is the scale up cost found using Equation 1 and BMC0 is the base cost. The Factored Estimated approach for the techno-economic analysis is utilized by Carrasco et. al. (2017). Heat duty calculations were completed for the process heater (electricity needed to heat) and the cooling water needed to cool down the that needs to enter into the PEC reactor at 25 °C.

$$1.18*\Sigma BMC + 0.5*\Sigma BMC0$$ **Equation 2**

The return on investment (ROI) was calculated as the net earnings (accounting for multiplier of 40% since taxes will be taken out) divided by the cost total capital investment (CTCI). Table **35** provides a snapshot of the calculation for when an ROI is assumed to be 10%. At an ROI of 10%, the plant needs to make at least $8.2M in sales.

Table 35. Return-on-Investment

ROI		0.1	assumed
net earnings	$	8,219,858.54	$/year
CTCI	$	58,713,275.32	
CTPI	$	51,201,924.23	
CWC		$7,511,351.09	
CTPI eqn	$	51,201,924.23	
CDPI	$	45,291,401.30	
land	$	1,250,000.00	
royalties		$1,593,418.06	
startup		$3,067,104.87	
CTBM (BMC)	$	41,174,001.18	

Minimum Fuel Selling Price and Higher Heating Value

The minimum fuel selling price (MFSP) quantifies the cost of the lowest price needed for the fuel to sell at a profit on the overall investment of the plant. **Table 36** shows the calculated MFSP for the bio-fuel with respect to the full EDOx process alone and is independent of upstream and downstream operations. Note that annual production rate is over 1.11 M gal of product (bio-fuel) per year. This is due to a large recycle stream that is from downstream operations (after full EDOx process section) in the overall simulation. Thus, for the MFSP value it was assumed to be an annual production rate of 1.11M gal of bio-fuel product per year.

Table 36. Minimum Fuel Selling Price for EDOx Upgrading Segment

MFSP breakdown			
	$/gal product		
Feedstock	0.067880682	Feedstock	**$7,555,500.00**
Maintenance + overheads	0.032046295	Maintenance + overheads	$3,566,932.11
Utilities	0.013950051	Utilities	$1,552,718.82
Average IRR	0.95	Average IRR	used Carrasco input
Capital Depreciation	0.42	Capital Depreciation	used Carrasco input
Average income tax	0.35	Average income tax	used Carrasco input
Catalyst	0	Catalyst	0
Distribution & selling	0.003686626	Distribution & selling	$410,342.17
Operating Labor	0.006766955	Operating Labor	$753,200.00
Others	0.04906085	Others	$5,460,747.29
Waste treatment	0	Waste treatment	0
MSP ($/gal)	1.89339146		
MSP*	1.720173391		
* at actual annual production of 111,305,599,472			

Conclusions of TEA/LCA Activity

Techno-economic analysis (TEA) and life cycle analysis were also conducted. Results show that the EDOx configurations have lower life cycle GHG emissions of 5 – 8.4 g CO_2 eq. and 7.4 – 11 g CO_2 eq. per MJ of a vehicle operated with diesel and gasoline, respectively compared to HDO (39 gCO_2 eq. per MJ). Furthermore, the EDOx process offers potentially10 times more small-scale pyrolysis upgrading facilities in the U.S. compared to HDO, suggesting that small-scale on-site EDOx processes can reach more inaccessible forest biomass resources.

The plant is designed to use 300 metric tons/day of forest residue to produce 1.1 M gallons per year of gasoline and diesel which is an overall yield of 47 L of fuel produced per dry metric ton of feedstock. The processing steps include:

1. Feedstock collection
2. Fast pyrolysis conversion of feedstock to bio-oil
3. Electrochemical deoxygenation of bio-vapor to produce stable deoxygenated oil

4. Further hydrotreating of electrochemical deoxygenated oil

5. Product separation of deoxygenated oil

The capital cost for the plant is estimated to be $53 million (2015 basis). At an ROI of 10%, the minimum fuels (gasoline and diesel) selling price is $1.89/gal which is competitive with the estimated MFSP of the state of the art HDO technology reported to be between the range of $1.74- $2.04/gal. In addition we project that the revenue from sales of the biofuel product at the estimated MFSP will be $210 million.

Although the MFSP of the EDOx process is relatively competitive with the HDO technology, the EDOx process has the potential to have a lower MFSP if the EDOx reactor can reach its full deoxygenation potential, thereby reducing the hydrogen demand required for further deoxygenation and reduce cost. Therefore, further research can possibly lead to additional cost improvements.

References – TEA/LCA

Carrasco, J. L.; Gunukula, S.; Boateng, A. A.; Mullen, C. A.; DeSisto, W. J.; Wheeler, M. C., Pyrolysis of forest residues: An approach to techno-economics for bio-fuel production. *Fuel* **2017,** *193*, 477-484.

Dutta, A., et al., *Process Design and Economics for the Conversion of Lignocellulosic Biomass to Hydrocarbon Fuels. Thermochemical Research Pathways with In Situ and Ex Situ Upgrading of Fast Pyrolysis Vapors*. 2015, NREL (National Renewable Energy Laboratory (NREL), Golden, CO (United States)).

Han, J., Elgowainy, A., Palou-Rivera, I., Dunn, J.B. Wang, M. Q., Well-to-Wheels Analysis of Fast Pyrolysis Pathways with GREET. Argonne National Laboratory: Oak Ridge, Tennessee, 2011, http://greet.es.anl.gov/publication-wtw_fast_pyrolysisp 76.

Hsu, D. D., Life cycle assessment of gasoline and diesel produced via fast pyrolysis and hydroprocessing. *Biomass Bioenergy* **2012,** *45*, 41-47. DOI: http://dx.doi.org/10.1016/j.biombioe.2012.05.019

International Organization for Standardization, ISO 14041: Environmental Management: Life Cycle Assessment- Goal and Scope Definition and Inventory Analysis. Geneva, 2006, https://www.iso.org/standard/23152.html.

James, B.D., Baum, G.N., Perez, J., Baum, K.N., 2009. Techno-economic analysis of photoelectrochemical (PEC) hydrogen production, Directed Technologies, DOE Contract Number: GS-10F-009J, Deliverable Task 5.1: Draft Project Final Report, Arlington, VA.

Jones, S. B.; Holladay, J.; Valkenburg, C.; Stevens, D.; Walton, C.; Kinchin, C.; Elliott, D.; Czernik, S. *Production of Gasoline and Diesel from Biomass via Fast Pyrolysis, Hydrotreating and Hydrocracking: A Design Case* PNNL-18284; 2009; p 76.

Milobar, D. G.; Hartvigsen, J. J.; Elangovan, S., A techno-economic model of a solid oxide electrolysis system. *Faraday Discussions* **2015,** *182*, (0), 329-339.

Pre Consultants *SimaPro V. 8.1.1.16*, 8.1.1.16; PRé Consultants: The Netherlands, 2014.

Sorunmu, Y., Billen, P., Elangovan, E., Santosa, D., Spatari, S., Life cycle assessment of alternative pyrolysis upgrading systems: implications of configuration, scale and hydrogen requirement, *ACS Sustainable Chemistry & Engineering* **2018**, (in review).

Torelli, M., Billen, P., Spatari, S., 2018. Techno-Economic Analysis of EDOx Pyrolysis Bio-oil Upgrading, manuscript in preparation.

US DOE, 2006. United States Department of Energy - Office of Energy efficiency and Renewable energy, Biomass Feedstock and Composition Database.

Wang, 2015. GREET (The Greenhouse Gases, R. E., and Energy Use in Transportation Model) Argonne National Laboratory: Argonne, Illinois.

Chapter 4. Research Opportunities

The potential of deoxygenating bio-oil with an integrated electrochemical device has been demonstrated. The solid oxide electrolysis device that was used is designed and its electrodes optimized for 800 °C operation. For physical and process integration the electrochemical device needs to be operated at 550 °C or below. Such low operating temperature significantly reduces the performance of the electrolysis device. The current density of the electrolysis unit, and correspondingly its oxygen transporting ability, is only about 5 to 10% of its capability at 800 °C. This project demonstrated a thin electrolyte cell design that showed improved performance at the lower temperature when tested in a button cell. Thin electrolyte design with its increased performance will reduce the capital cost of the device. More research is needed to evaluate fuel electrode (cathode) material with higher catalytic activity and oxygen electrode material with lower polarization losses.

A second aspect work that needs additional research and demonstration is larger scale stack that can receive all of the pyrolysis vapor for deoxygenation study. In the present project, a 10-cell stack was able to receive and process 10% of the vapor from the experimental pyrolysis unit. Analysis showed that nearly 40% deoxygenation occurred. With a projected five-fold increase in performance with the use of thin electrolyte, a stack of 100 cells would theoretically remove a significant amount of oxygen.

Integration of the two devices, pyrolyzer and the electrolyzer, needs further study and optimization.

First principle modeling needs to further extended to identify a suitable catalyst that can be either used as the cathode or incorporated into it to improve deoxygenation capability and to improve selectivity of desired product.